1-1-1998

TCSC controller design to damp interarea oscillations

Ning Ning
Iowa State University

TCSC controller design to damp interarea oscillations

by

Ning Yang

A thesis submitted to the graduate faculty

in partial fulfillment of the requirements for the degree of

MASTER OF SCIENCE

Major: Electrical Engineering

Major Professor: Dr. James D. McCalley

Iowa State University

Ames, Iowa

1998

Graduate College
Iowa State University

This is to certify that the Master's thesis of

Ning Yang

has met the thesis requirements of Iowa State University

Signatures have been redacted for privacy

To my parents

TABLE OF CONTENTS

LIST OF TABLES

LIST OF FIGURES

ABSTRACT

Thyristor Controlled Series Compensator (TCSC) is a prominent Flexible AC Transmission System (FACTS) device. It can control the transmission line impedance quickly and widely. It results in significant improvement for both power system steady state and dynamic issues. The goal of this thesis is to design a TCSC controller to damp interarea oscillations in a power system.

A traditional controller design method, called the residue method, used to design power system stabilizers (PSS), is used to design the TCSC controller. The controller designed by this method yields good damping results. This method, along with modal sensitivities, is also used to indicate the effectiveness of various TCSC locations. The performance of TCSC and PSS controllers are compared for different static load modeling. The results indicate that TCSC has great influence on both interarea modes of the sample system relative to the influence of PSS. Also TCSC has the potential to improve one interarea mode and degrade the other. This suggests that controller robustness is of greater concern with TCSC than with traditional power system controllers. To account for this, the uncertainties in static load modeling are modeled into structured uncertainties, and we utilize the μ analysis and synthesis to design a robust TCSC controller. This controller has low order and can work well under different static load modeling. This controller design scheme is practical in the sense that it can adapt to a wider range of system parameters without increasing too much in complexity.

CHAPTER 1 INTRODUCTION

1.1 The need for FACTS controllers in AC system

1.1.1 What is FACTS?

FACTS, the acronym of Flexible AC Transmission System, has been defined by the IEEE as "alternating current transmission systems incorporating power electronic based and other static controllers to enhance controllability and increase power transfer capacity" [1]. The controllers are called FACTS devices.

Generally, because of the nature of power electronics, a FACTS device will demonstrate one of the following features:

- rapid response
- frequent variation of output
- smoothly-adjustable output

Research institutions, utilities, and manufacturers throughout the world are pursuing programs with two main objectives [1]:

- to increase the power transfer capability of transmission networks
- to provide direct control of power flow over designated transmission routes

These objectives have been addressed by electric utilities over their entire history. Until recently, however, adding generation and transmission in judicious locations provided

most of the desired capability. Now, however, the current environment of deregulation and constraints on building more transmission facilities provides compelling reasons to develop alternative approaches. Mature power electronic based FACTS equipments can be considered a dependable means to help achieve these goals.

1.1.2 Power transfer limitations and solution by using FACTS

Technically, limitations on a power system can be relieved by installation of new transmission facilities. However there are many impediments today to constructing new facilities. So in the discussion below, we will assume that is not a viable option.

The limitations of power system transfer capacity can be summarized into two categories, steady state issues, including voltage limits and thermal limits; and dynamic issues, including transient stability, damping, sub-synchronous resonances, and voltage stability. Such limitations and corrective controls provided by FACTS devices are listed in Tables 1.1 and 1.2:

1.1.3 Demand of FACTS by the restructured power industry

Electric power utilities are undergoing significant restructuring in many countries. The trend started in the 1980's in the UK and Chile. In the U.S., where the electric utility industry is for the most part owned by the private sector, the drivers have been customer choice, increased competition and reduced regulation. Large energy customers along with energy brokers have been placing immense pressure on federal and state government for full competition in wholesale and retail energy sectors. The Federal Energy Regulatory Commission(FERC) and state regulator have taken a series of initiatives to create competitive energy markets as a result of these pressures.

In 1995, the California Public Utilities Commission (CPUC) ordered the restructuring of the electric utility industry in California to allow full competition in the retail and wholesale electricity markets starting in January 1998. Under the plan, two completely

Table 1.1 Steady state issues

Issue	*Problem*	*Corrective action*	*FACTS solutions* [a]
Voltage limits	Low voltage at heavy load	Supply reactive power	TCSC, SVC STATCOM
	High voltage at light load	Remove reactive power supply	TCSC, TCR
		Absorb reactive power	TCR, STATCOM
	High voltage following outage	Absorb reactive power	TCR
		Protect equipment	TCVL
	Low voltage following outage	Supply reactive power	STATCOM, TCSC
		Prevent overload	IPC, TCPAR TCSC
	Low voltage and overload	Supply reactive power and limit overload	TCSC, UPFC, STATCOM
Thermal limits	Line/transformer overload	Reduce overload	TCSC,TCPAR, UPFC
	Tripping of parallel circuit	Limit circuit loading	IPC, UPFC, TCR

[a]TCSC = Thyristor Controlled Series Capacitor
IPC = Interphase Power Controller
STATCOM = Static Synchronous Compensator
SVC = Static Var Compensators
TCPAR = Thyristor Controlled Phase-angle Regulator
TCR = Thyristor Controlled Reactor
TCVL = Thyristor Controlled Voltage Limiter
UPFC = Unified Power Flow Controller

independent and not-for-profit organizations called the Power Exchange (PX) and the Independent System Operator (ISO) would be created to facilitate the operation of the competitive energy market in California. The PX will conduct competitive energy auction, and develop energy schedules based on the result of this auction. The ISO will coordinate the energy schedules provided by the PX with the schedules of other market participants (called schedule coordinators or SCs), operate the power transmission system, and settle/bill for the deviations that occur between the planned and actual schedules.

Under these competitive circumstances, major changes in the system configuration via construction of new transmission facilities is extremely unlikely. Therefore, power system facilities are and will continue to be operated very close to their limits. Also

Table 1.2 Dynamic issues

Issue	*Type of system* [a]	*Corrective action*	*FACTS solutions*
Transient stability	A, B,D	Increase synchronizing torque	TCSC, UPFC
	B,C,D	Dynamic flow control	TCPAR,UPFC, TCSC
Damping	A	Damp 1 Hz oscillations	TCSC, STATCOM
	B,D	Damp low frequency oscillations	SVC,TCPAR, UPFC, TCSC,STATCOM
Post-contingency voltage control	A,B,D	Dynamic voltage support	STATCOM, UPFC,SVC
		Dynamic flow control	STATCOM, UPFC
		Dynamic voltage support and flow control	UPFC, TCSC,SVC
	A,B,C D	Reduce impact of contingency	TCSC,STATCOM, IPC,UPFC
Voltage stability	B,C,D	Reactive support	STATCOM, UPFC
		Network control actions	UPFC,IPC, TCSC,STATCOM
		Load control	Demand-side management programs

[a]A. Remote generation - radiial lines
B. Interconnected areas
C. Tightly meshed network
D. Loosely meshed network

because of the competition, congestion is likely to occur on the paths connecting the inexpensive energy and load centers. Moreover, the PX market is unpredictable. Power system operating conditions may change dramatically from hour to hour. In order to avoid high wheeling charges, loop control is required. Therefore, control is required to relieve the constraints and therefore increase available transfer capacity as close as possible to the thermal limits. These control are also desirable so as to directly control the line power flows quickly and effectively. FACTS device can well serve this purpose.

1.2 Brief description of TCSC

1.2.1 Introduction

By adjusting series impedance, power flow can be guided to the desired branches or areas. One of the commonly used methods is to install series capacitors. The series impedance is then reduced. The use of series capacitors in this manner is called series compensation. It provides that the power transfer capacity between areas can be increased and additional power flow can be scheduled.

Conventional series compensation schemes employing mechanical switching have been studied a great deal. By introducing power electronics, a new series compensation scheme, which is called Thyristor Controlled Series Compensator(TCSC), can greatly improve the system characteristics in terms of system damping, first swing stability, and increased power flow.

By merging conventional series capacitor components with solid-state power technology, TCSC demonstration projects have been placed in operation at Kayenta Substation [2] and Slatt Substation [3] in the USA, according to [4]. The technical benefits derived from these projects include:

- Flexible, continuous control of transmission line series compensation level
- Direct dynamic control of power flow within the network
- Damping of local and interarea oscillations (power swings)
- Short circuit current reduction
- Subsynchrous resonance (SSR) mitigation
- Improved component protection

1.2.2 Module of TCSC

A TCSC module consists of a series capacitor with a parallel path including a thyristor switch with surge inductor, as shown in Fig. 1.1. Also included is a Metal-Oxide Varistor (MOV), which will break down under over-voltage to provide protection, and a bypass breaker to switch in or out the TCSC module. By changing the magnitude, even the direction of the circulating current (I_T in Fig. 1.1), the apparent impedance (V_C/I_{Line}) of the module will change significantly.

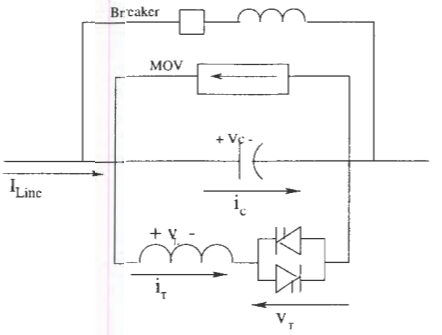

Figure 1.1 Single module TCSC circuit

A complete TCSC system may be comprised of several such modules in series, and it may accompany a conventional fixed series compensator bank as part of an overall project, as shown in Fig 1.2, to aid power system performance.

TCSC power circuits have three modes of operation:

1. Thyristors blocked (no gating and zero thyristor current)
2. Thyristors bypassed (Continuous gating and full thyristor conduction)
3. Vernier mode operation with phase control of gate signals and consequent partial thyristor conduction.

When the thyristors are blocked, the power circuit impedance is the fundamental frequency capacitor reactance; when the thyristors are fully conducted, most of the line current flows through the thyristor path and the TCSC has a net inductive impedance.

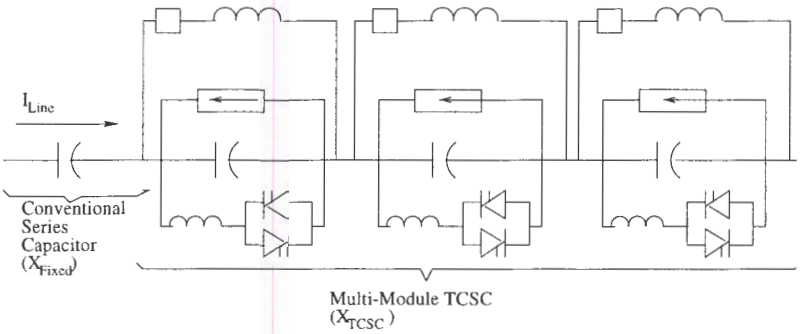

Figure 1.2 Multi module TCSC circuit

For the vernier mode operation, when the module is operating with low levels of thyristor conduction, circulating current, which is produced by accumulated charges across the capacitor (the capacitor accumulates the energy so that it raises its voltage), effectively boosts the fundamental frequency voltage across the capacitor segment resulting in a capacitive impedance greater than the nominal. When the modules are operating with high levels of thyristor conduction, the circulating current is reversed and the net impedance will be inductive at the fundamental frequency. Vernier operation has the benefit of virtually enlarging the series compensation level. However, it also has implication on the ratings of capacitor, the reactor, and the thyristor valves.

1.2.3 Benefit of TCSC

Series compensation is a well-established technology as an economical means for increasing the power transfer capacity of transmission lines and for controlling power flows on parallel transmission corridors. Series capacitors are mainly installed in transmission systems to solve the following problems:

- Low capacity usage of transmission lines due to the flow of less than the scheduled amount across a transmission corridor, which is caused by loop flow. It can impact system security, especially following a critical line outage.

- Transient instability problems exhibited by loss of synchronism following major disturbance.

- Instability characterized by negatively damped low frequency oscillations. This situation arises when a high level of power is transmitted over a weak transmission link. Negatively damped oscillations can arise in the steady state or this can arise following large disturbance.

- Voltage instability problems exhibited by a slow decline of the voltage profile with increases in power loading of the transmission circuits. Series capacitors compensate some of the reactive losses in a transmission circuit, and they are self regulating in that the amount of reactive power generated increases with the loading level of transmission circuit. This facilitates control of the local network voltages.

The level of installed series compensation has traditionally been limited due to concerns of subsynchronous resonance (SSR). SSR is exhibited by a slow buildup of energy exchange between the electrical system and the shaft of a nearby turbine-generator which leads to fatigue and possible failure of the generator shafts. There are other constraints such as thermal rating and overall losses.

Thyristor Controlled Series Capacitor (TCSC) enhances the benefits to the power system associated fixed capacitor and offer additional ones as well. Some of the TCSC benefits are described in the remaining of this subsection.

1.2.3.1 Power transfer capacity improvement and loop flow control

TCSC offers the flexibility of varying the level of inserted series compensation in order to increase the power flow over the compensated lines. This allows the operator to shift power flow to desired high-voltage lines which results in decreased losses and relief of overload of low-voltage lines. Phase shifters can also offer the flexibility of line power flow control.

For any interconnected power system, power may flow to unscheduled routes. Direct control of line impedance provided by TCSC can guide the power flow to the desired route and therefore avoid additional wheeling charges.

1.2.3.2 Transient stability improvements

Series compensation can shorten the electrical distance between the generators connected to the compensated lines. This may increase the synchronizing torque and result in the improvement of transient stability.

We can alleviate the severity of a transient instability problem if we can increase the compensation level for the first swing and the inductive compensation for the return swing. The maximum compensation level of TCSC is determined by the rating of the capacitor. With the TCSC installed, during the immediate period after fault, we can use the short time rating of capacitor, which means greatly increased compensation level.

1.2.3.3 Subsynchrous resonance mitigation

TCSC has the ability to control the energy interchange between a series capacitor and a generator-turbine shaft [4]. So it is possible to increase the level of compensation without the risk of potential SSR problems. TCSC is able to mitigate SSR and provide SSR-free series compensation systems. This will enable the application of series compensation in portions of the transmission network for which is has never before been possible.

1.2.3.4 System damping improvement

The power system often experiences low frequency (below 1 Hz) interarea oscillations when the power transfer between two areas exceeds a threshold. One thing that determines the threshold is the strength of the interconnecting transmission systems. A small segment of capacitor (e.g. $\pm 10\%$) is sufficient to damp power system oscillation.

By using some local measurement feedback control, TCSC can offer the possibility of dramatically improved damping of power oscillations and increased levels of stable power transfer between two regions.

1.2.4 TCSC controller for damping

TCSC reactance can be continuously varied between capacitive and inductive. Under these modes, TCSC has the potential to increase the damping by providing great impedance variation for the first swing and small variation for the others. One possible control to enhance stability is illustrated by the block diagram shown in Fig. 1.3. To improve damping, the line impedance must be modulated in harmony with the power swings. This can be achieved by properly designed controllers using the input signal as bus voltage or real power flow. The control block consists of two loops, one is a damping loop and the other is the synchronization loop. The synchronization loop has little delay and large range of variation of compensation level. It is used to achieve synchronization after a large disturbance. The synchronization loop acts initially after the disturbance, leading to the maximum compensation level during the adjustable time Ta. In sequence, the control is smoothly transfered to the damping loop, which has large delay and some variation of compensation level. It only acts to damp small swings when the system has been synchronized.

1.3 Problem statement

Among all of the benefits from TCSC, the damping control is the most attractive one. Low frequency interarea oscillations often exist in power system, and they can limit transfer capacity. Also, such oscillations are very hard to damp by conventional power system stabilizer (PSS). Because TCSC can be installed in the transmission circuit across which the energy oscillation occurs, it can be very effective in damping interarea

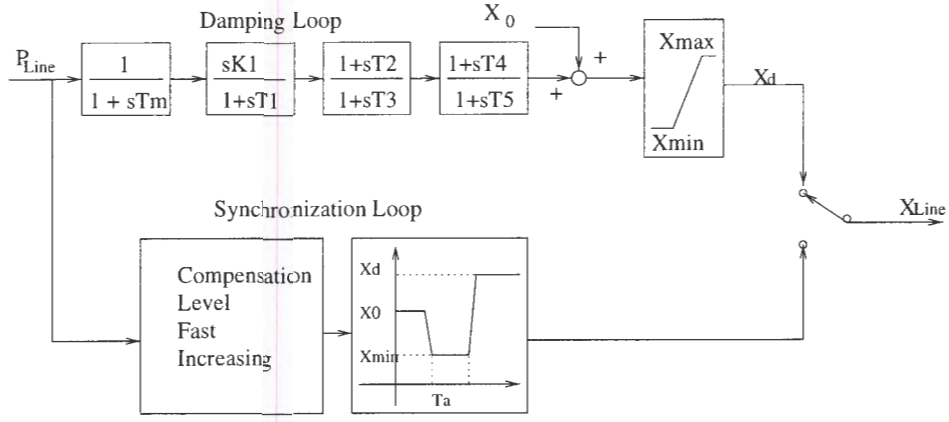

Figure 1.3 TCSC damping control block diagram

oscillation.

Significant attention has been paid to the TCSC model. Reference [5] presented a model which considers TCSC as a variable reactance. Reference [6] investigated the characteristics of TCSC. References [7] and [8] gave the transfer function of TCSC, but these functions are different. So at the beginning of this work, we illustrate in detail the operating procedure of TCSC. Then we investigate the relationship between transient response and steady state response. In addition, we develop the the transfer function between the thyristor firing angle and reactance.

Different control methods and signals [9, 10] have been applied to TCSC to damp system oscillations. The method presented in this research is based on functional sensitivity (i.e., residue method) [11] from small signal stability analysis. This method performs eigenvalue placement using the residue. It was applied to PSS in [12, 13, 14]. But TCSC, as are most of the FACTS devices, is installed in a transmission line, in contract to PSS which is installed in a generator. Intuitively we think that TCSC has a more global effect than PSS, i.e., TCSC has greater potential than PSS to affect system global behavior dramaticaly, either improving or degrading. Therefore, robustness for TCSC design may be more critical than for PSS design.

Reference [15] reports an informative investigation regarding the robustness issue.

It compared the modal controllability between three kinds of FACTS device and PSS. It is shown that the direct contribution of the FACTS-based stabilizer is through all the generators in the power system, while that of PSS is merely through the generator where it is installed. It concluded that the robustness of FACTS-based stabilizers to the changes of the configuration and operating conditions of power system is as poor as, or even poorer than, that of the PSS. But the input signal, i.e. the modal observability, also has great influence on controller performance. So we use the functional sensitivity instead of modal controllability to compare the robustness of TCSC and PSS.

It is known that load representation has great influence in power system stability [16, 17]. Errors in modeling can destabilize a well damped system. But accurate coefficients of load modeling are hard to obtain. Also, these coefficients are subject to change from time to time. The influence of these uncertainties on controller design is illustrated by the comparison of PSS and TCSC, which are designed by the residue method.

Conventional power system controller design uses the linearized system model. It depends greatly on the operating point. When we design a controller under certain load representation, it may not be effective or perhaps it may even degrade the system for another set of coefficients. Therefore some design method is required to account for the uncertainties in the coefficients in load representation.

The idea of robust control is developed to deal with the situation that the system has modeling errors or wide range of operating point. These uncertainties can be modeled as a block matrix that connect some vector of output to the some input. This block matrix is called uncertainty block. According to the structure of this uncertainty block, the uncertainties can be formulated into two categories, one is unstructured uncertainties, the other is structured uncertainties. For the structured uncertainties, different input/output pairs that connected to the uncertainty matrix is decoupled, i.e., the uncertainty block is diagonalized; but the unstructured uncertainty matrix may not has such special structure [18]. Also, such uncertainties can be considered as linear or non-

linear, depending wheather the transferfunction that connect the uncertainty block is linear or nonlinear.

Some research has been done to apply the robust control to power system controller design. Most of these works deal with the unstructured uncertainties [19, 20, 21] in load level (but not load composition). The result is relatively conservative, since the uncertainty block can only be considered as a full matrix. Paper [22] forms the uncertainties in line susceptance into structured uncertainties in order to simulate the uncertainties in line power flow, and paper [23] treats the uncertain coefficients in the linearized generator diagram as structured uncertainties in solving the problem of uncertain load level. When the structure of uncertainties is known, we can utilize such special structure to design the controller which is less conservative. Such analysis and controller design is called μ analysis and synthesis.

This research tries to utilize this method to analyze linear problem. It represents static load as the composition of constant impedance, constant current and constant power and considers the uncertainties as the proportion of such load composition. Under the condition of small signal stability and without changing the load level, such uncertainties are linear in terms of the deviation of bus voltage and they can be formulated as the structured uncertainty. Then we use μ analysis to study the effect of such uncertainties on small signal stability. Since there is no approximation in the formulation of uncertainties, it is possible to design a controller that is relatively low order but also has control influence that is relatively unaffected by the variation in load modeling.

1.4 Thesis organization

In Chapter 2, the transient behavior of TCSC is studied and the relation between thyristor firing angle and apparent impedance is identified. A general controller design method is illustrated in Chapter 3, which can be applied to a controller design of different

input/output pairs. This design method is applied to TCSC. The siting problem is also discussed in this chapter. In Chapter 4, a comparison is made for the damping performance of PSS and TCSC with uncertainties in load representation. In Chapter 5, the uncertainties in load representation is modeled as structured uncertainties. And μ analysis and synthesis are performed to TCSC in this chapter. The conclusion is summarized in Chapter 6.

CHAPTER 2 MATHEMATICAL DESCRIPTION OF TCSC

2.1 Introduction

TCSC is a fairly new FACTS device. It only has two installation examples. Also there are not too many papers illustrating the detail of TCSC modeling [7, 8]. Moreover, these papers are not consistent. In this chapter, we will investigate TCSC operation to understand the device, especially the relation between the firing angle of thyristor and apparent impedance. We emphasize this relation because for TCSC, the controllable variable is the firing angle of the thyristors and the output is the apparent impedance.

Figure 2.1 shows the typical circuit of TCSC and defines the current and voltage. The discussion of this chapter follows these definitions. The impedance convention used here assumes the capacitive reactance is positive.

In this chapter, we use follow the common procedure to study the device. The steps are:

1. Obtain the transient description of TCSC operation by the Laplace transform.

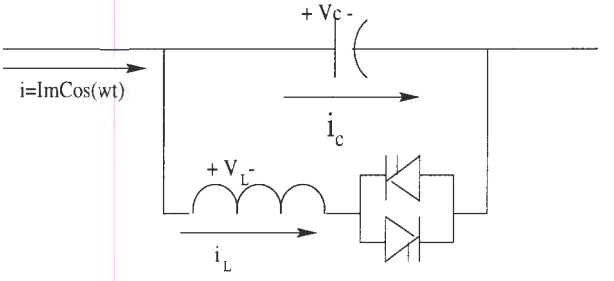

Figure 2.1 TCSC circuit

2. Obtain the steady state description of TCSC, based on observation of steady response of the device.

3. Obtain the formular of steady state compensation of TCSC. Then, by fourier expansion, obtain the transfer function of firing angle and apparent impedance of TCSC at the fundamental frequency, since TCSC is going to be used in the study of power system behavior in the fundamental frequency.

There are some simulation result following each step to verfy the validity.

2.2 Step 1: transient operating procedure TCSC

When the firing angle of the thyristors of TCSC changes, the capacitor voltage will experience a transient procedure before reaching steady state. An equivalent circuit for the TCSC is shown in Figure 2.2, where the line current is represented as an ideal current source and the thyristor is replaced with a switch K.

When we consider the mode of switch, it has two operating modes: one is open, the other is close. These correspond to the status of thyristor which is either open or blocked, as in Figure 2.2 where switch K is open or closed. The transient can be derived for each mode of the switch. The firing angle α is defined as the delay angle after thyristor

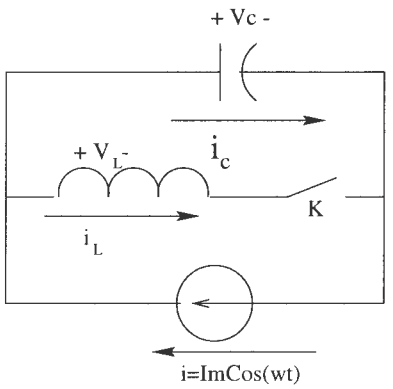

Figure 2.2 Equivalent circuit

is positive biased.

2.2.1 Thyristor blocked

When K turns off in Figure 2.2, the voltage of capacitor at that time is denoted as V_{c1}, and the phase angle at that time is denoted as β, which is the relative angle according to the zero-crossing of line current. From this situation, the following differential equations can be obtained.

$$\begin{aligned} C\frac{dv_c}{dt} &= i_c \\ i_c = i &= I_m \cos(\omega t) \\ v_c(t = \frac{\beta}{\omega}) &= V_{c1} \end{aligned} \tag{2.1}$$

You may directly solve these differential equations, or use Laplace and inverse Laplace transform. Solution of these differential equations yields,

$$\begin{aligned} i_c &= i = I_m \cos(\omega t) \\ i_L &= 0 \\ v_c &= \frac{I_m \sin(\beta)}{\omega C} - \frac{I_m \cos(\beta)\sin(\omega t - \beta)}{\omega C} - \frac{I_m \sin(\beta)\cos(\omega t - \beta)}{\omega C} + V_{c1} \end{aligned} \tag{2.2}$$

These equations are valid when $\beta < \omega t < \alpha$.

2.2.2 Thyristor conducting

When the thyristor is triggered at α, it is conducting, with switch K closed in Figure 2.2. At that time the voltage of the capacitor is V_{c2}. From Figure 2.2 the following

differential equations can be obtained.

$$\begin{aligned} C\frac{dv_c}{dt} &= i_c \\ L\frac{di_L}{dt} &= v_L \\ i_c + i_L = i &= I_m \cos(\omega t) \\ v_c(t = \frac{\alpha}{\omega}) &= V_{c2} \end{aligned} \tag{2.3}$$

By solving these differential equations, we obtain

$$\begin{aligned} i_L &= -A\cos(\omega t) + \sin(\omega_0 t)(-B\sin(\alpha)\cos(k\alpha) + A\cos(\alpha)\sin(k\alpha) + V_{c2}D\cos(k\alpha)) \\ &\quad + \cos(\omega_0 t)(B\sin(\alpha)\sin(k\alpha) + A\cos(\alpha)\cos(k\alpha) - V_{c2}D\sin(k\alpha))) \end{aligned} \tag{2.4}$$

$$\begin{aligned} v_c &= \frac{B}{D}\sin(\omega t) + \frac{1}{D}\cos(\omega_0 t)(-B\sin(\alpha)\cos(k\alpha) + A\cos(\alpha)\sin(k\alpha) + V_{c2}D\cos(k\alpha)) \\ &\quad + \frac{1}{D}\cos(\omega_0 t)(-B\sin(\alpha)\sin(k\alpha) - A\cos(\alpha)\cos(k\alpha) - V_{c2}D\sin(k\alpha))) \end{aligned} \tag{2.5}$$

where

$$\begin{aligned} A &= \frac{I_m\omega_0^2}{\omega^2 - \omega_0^2} \\ B &= \frac{I_m\omega_0\omega}{\omega^2 - \omega_0^2} \\ k &= \frac{\omega_0}{\omega} \\ D &= \omega_0 C \\ \omega_0 &= \frac{1}{\sqrt{LC}} \end{aligned} \tag{2.6}$$

The valid region for these equations is $\alpha < \omega t < \pi + \beta$

2.2.3 Simulation result

Assume L = 15mH, C = 212 μ F, I_m = 2kA, ω_0 = 561 and ω = 377 (60Hz), which is the same setting as the TCSC at Kayenta Substation [6]. In order to compare with

other docuemnts that describe this TCSC, α is assigned to be 133^0. The direction of voltages and currents are as Figure 2.1.

The steady state capacitor voltage and thyristor current are shown in Figure 2.3. The capacitor voltage and current for start-up, when the thyristors begin to gate from complete blocked at $t = 0$, are shown in Figure 2.4, where one can observe that the firing angle $\alpha = 133^0$. Here, we see that the TCSC reaches its steady state after about 6 cycles. In addition, we observe that the steady state magnitude of capacitor voltage V_c' is over two times that of the capacitor V_c when the thyristor is blocked, when $\alpha = 133^0$. The actual compensation level of the module, i.e., the apparent impedance of the TCSC, is the voltage of the module divided by the line current. Here we obtain over twice the module voltage for the same line current, so that the compensation level is almost twice of a fixed compensation whose capacitor has the same capacity of this TCSC module. From Figure 2.5, it is apparent that as the capacitor voltage increases while α decreases from 137 to 130. Therefore, as for this TCSC module setting, we can increase the compensation level by firing the thyristors at smaller angle.

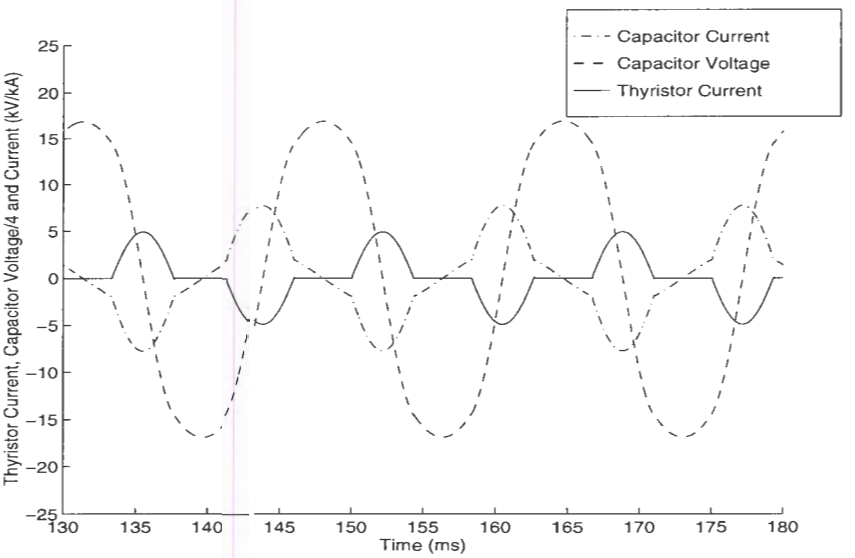

Figure 2.3 Steady state thyristor current, capacitor voltage and current

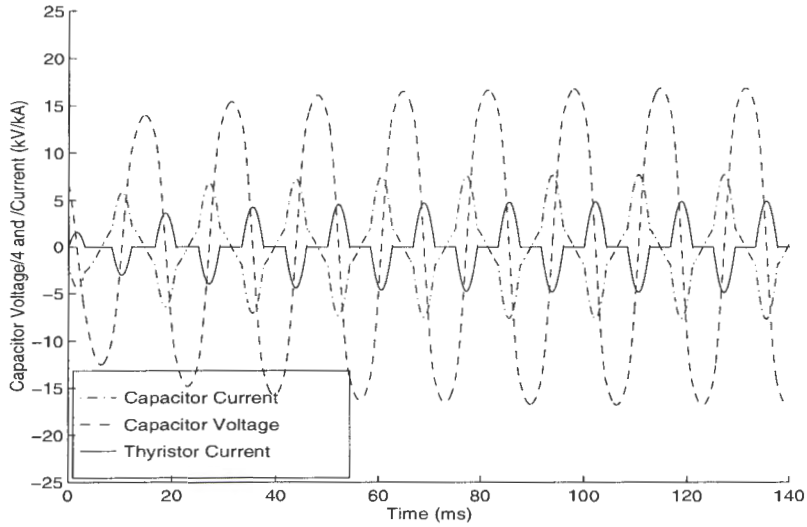

Figure 2.4 TCSC starting up

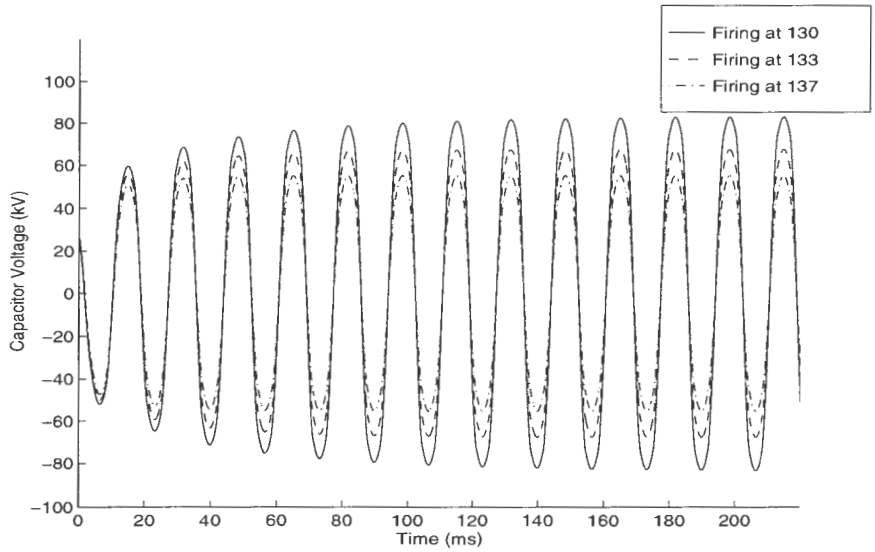

Figure 2.5 Different firing angle

2.3 Step 2: steady state description of TCSC

2.3.1 Steady state assumption

In the transient description of TCSC, we have the transition voltage V_{c1} and V_{c2}. In order to find the steady state description of TCSC, we need to make some assumption to eliminate these transition terms.

Assumption: from Fig. 2.3, we observe that in the steady state the thyristor current is similar to the line current (cosine) in symmetricity, i.e., the thyristor current is an even function of time, since we use a cosine line current to excite it. Therefore, there should be no sine components in the steady state current. Later on we will show the correctness of this assumption.

2.3.2 Steady state description of TCSC

For easy notation, we define σ as the conduction angle, $\sigma = \pi - \alpha$. Using this transformation, the thyristor current will be:

$$\begin{aligned} i_L = & - A\cos(\omega t) + \sin(\omega_0 t)(B\sin(\sigma)\cos(k\sigma) - A\cos(\sigma)\sin(k\sigma) + V_{c2}D\cos(k\sigma) \\ & + \cos(\omega_0 t)(B\sin(\sigma)\sin(k\sigma) + A\cos(\sigma)cos(k\sigma) - V_{c2}D\sin(k\sigma)) \end{aligned} \tag{2.7}$$

where A, B, k and D are defined in eqt. 2.6 and $-\sigma < \omega t < \sigma$.

Because we assume the thyristor current is an even function, the term associated with $\sin(\omega_0 t)$ need to be zero. Then we can solve the transition voltage V_{c2} and steady state thyristor current i_L as following:

$$\begin{aligned} V_2 &= \frac{A\cos(\sigma)tan(k\sigma) - B\sin(\sigma)}{D} \\ i_L &= -A\cos(\omega t) + \frac{A\cos(\sigma)}{\cos(k\sigma)}\cos(\omega_0 t) \end{aligned} \tag{2.8}$$

Figure 2.6 shows the transient current of thyristor (solid line) and the current (dashed line) calculated by steady state equations when $\alpha = 133$. It can be seen that the transient

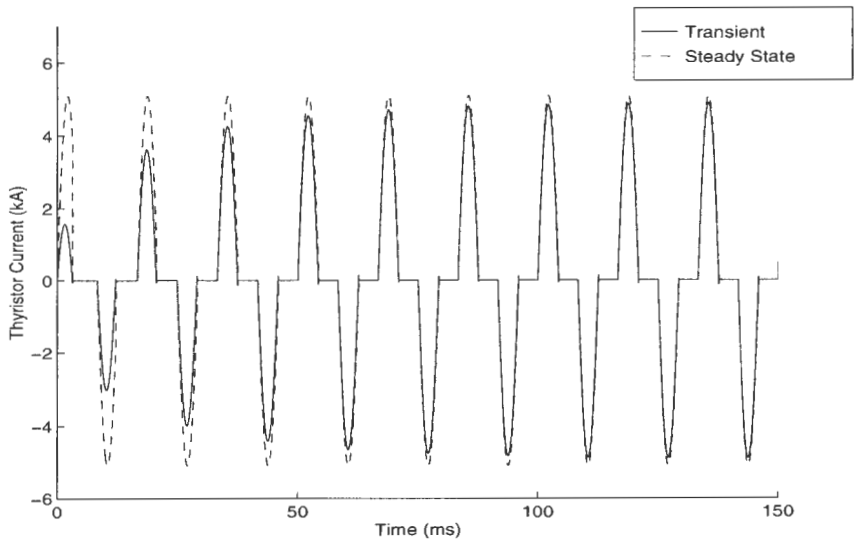

Figure 2.6 Effectiveness of steady state formula

is gradually approaching the steady state equations. This provides evidence that the assumption we have made that the steady state thyristor current is an even function is correct.

2.3.3 Properities observed from steady state description of TCSC

1. The currents when thyristor fires at another angle, $\alpha = 125^0$ are shown in Figure 2.7. The transient current needs more time to reach its steady state. But for this situation, we can get more reactive compensation. So in the practical application of TCSC, we need to accept a trade off between the response time and the amount of compensation.

2. Another interesting thing is the poles of the equation, where $\cos(k\sigma) = 0$. When thyristor is fired close to the poles, the current will not reach it steady state. It will become infinite until some protection acts. These poles are determined not only by firing angle, but also by ω_0, i.e. the structure of TCSC.

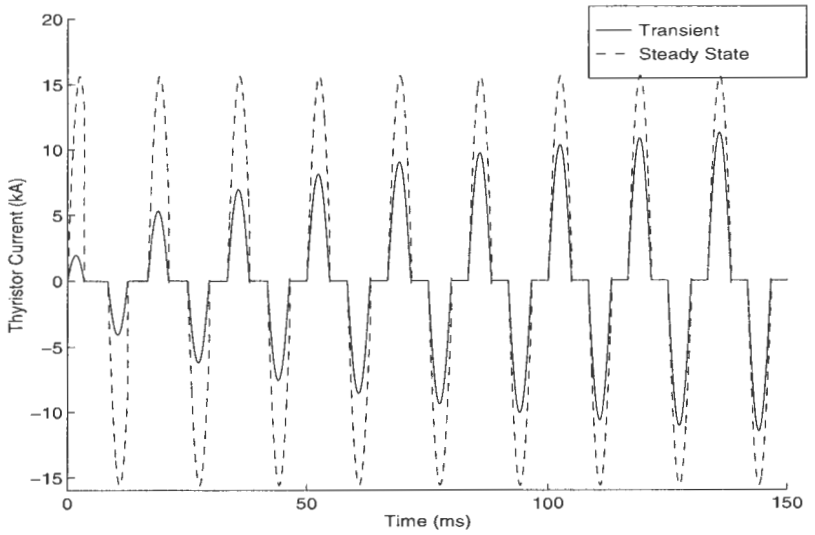

Figure 2.7 Relation between time constant and firing angle of TCSC

2.4 Step 3: steady state compensation of TCSC

The compensation impedance X which is defined as v_c/i_{line} can be calculated as:

$$\begin{aligned} X &= \frac{v_c}{i_{line}} = \frac{1}{\omega C}\frac{i_{line}+i_L}{i_{line}} \\ &= \frac{1}{\omega C} + \frac{1}{\omega C}\frac{i_L}{i_{line}} \end{aligned} \tag{2.9}$$

For most cases, we will study the behavior of the power system in fundamental frequency. By applying Fourier expansion to the steady state result in eqt. 2.9, the compensation of fundamental frequency, i.e. the coefficient of Fourier Series when n=1, is given as:

$$X_1 = \frac{1}{\omega C} + \frac{A}{\pi\omega C}[\sin(2\sigma)+2\sigma] + \frac{4A\omega\cos^2\sigma}{\pi C(\omega^2-\omega_0^2)}[k\tan(k\sigma)-\tan(\sigma)] \tag{2.10}$$

where $I_m = 1$ when A is computed.

To show the validity of eqt. 2.10 of impedance, it is applied to the same TCSC parameters as in section 2.2.3. The voltage calculated by $V = X_1 I$ is represented by the dashed line, and it is plotted with the exact voltage curve from Figure 2.3. Figure 2.8

shows that equation 2.10 gives a close approximation of reactance of TCSC. The relation between σ and reactance X_i is shown in Figure 2.9. There is an unreachable region around zero reactance. For σ that makes $k\sigma = \pi$, the reactance curve goes to infinite. It shows that we can reach much higher compensation level near this pole. The reactance curve is not only related to σ, but also to L and C. For another system configuration as in [7], $C = 177\mu F$ and $L = 3.4mH$, the reactance curve is shown in Figure 2.10.

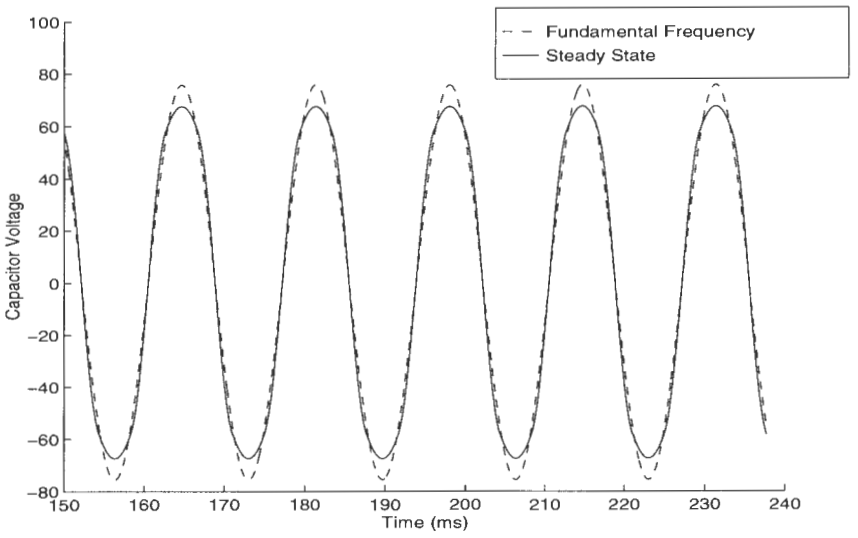

Figure 2.8 Impedance of fundamental frequency of TCSC

2.4.1 Transfer function of TCSC

When the time TCSC need to reach its steady state after the disturbance is considered, we approximate the time response of TCSC with one time constant T. Then the transfer function of TCSC can be written as:

$$X(s) = X_1 \frac{T}{sT + 1} \tag{2.11}$$

where T is the time constant and x_1 is calculated in Equation 2.10. It is under the assumption that the influence of higher frequency can be neglected. Also this equation may be expressed in p.u which assume the base of reactance as $\frac{1}{\omega C}$.

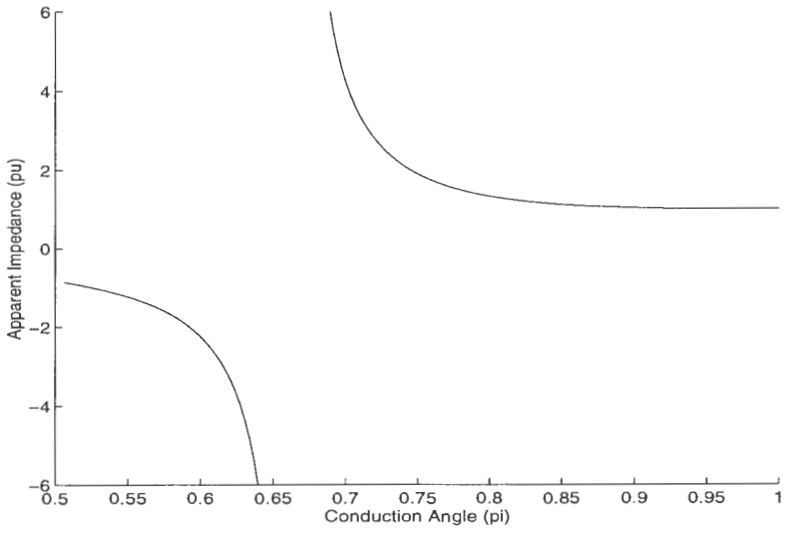

Figure 2.9 Relation between σ and Z of TCSC

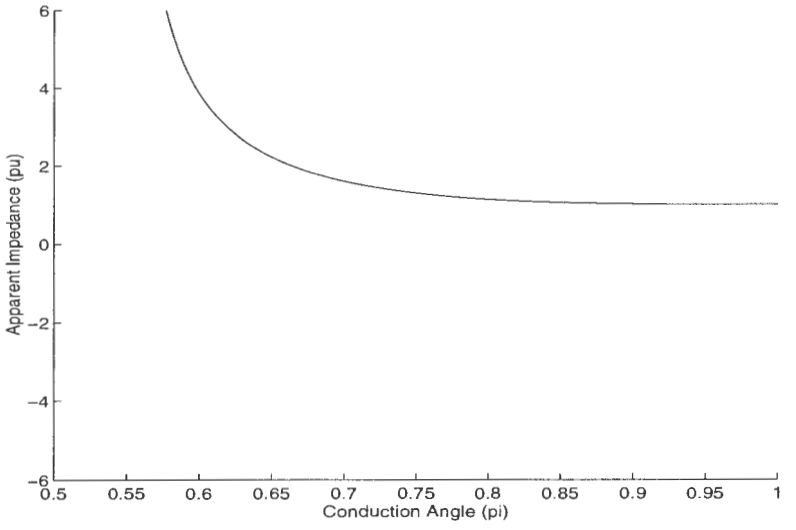

Figure 2.10 Another reactance curve of TCSC

T is the function of σ, L and C. In practical use, the range of the reactance is relatively small. For the sample module mentioned in section 2.2.3, when the reactance changes from 1.5 p.u. to 2.3 p.u., i.e. the firing angle changes from 131 to 136, T is between 13 ms and 18 ms. The commonly used value of T is 15 ms.

2.5 Conclusion

This chapter studies the transient and steady state behavior of TCSC. It provides the relation between thyristor firing angle and apparent impedance of the TCSC module. This relation is developed under the assumption that the components of higher frequency are negelectable. When it is applied to controller design to dampen power system oscillation, especially for low frequency inter-area oscillation, the time constant T can be neglected. Then the transfer function of TCSC can be simplified to an algebraic equation as in eqt. 2.10.

CHAPTER 3 TCSC CONTROLLER DESIGN FOR DAMPING INTERAREA OSCILLATIONS BY THE METHOD OF RESIDUE

3.1 Introduction

In the early days of interconnected power systems, generator loss of synchronism in the first few seconds following a fault was of great concern. This problem has been improved by the introduction of automatic voltage regulators (AVRs) and other technologies. But one side effect of AVRs is that it may reduce the damping torques and make the system more prone to oscillatory instability. This type of problem can be analyzed by linear system theory. The use of special techniques for linear dynamic analysis, applied to linearized system models, gives information on both the nature of oscillatory instability and on controls which can be used to eliminate the instability [16]. This method is called small signal stability analysis.

Damping of electro-mechanical oscillations between interconnected synchronous generators is necessary for secure system operation. A large power system has numerous modes of oscillation. These modes can be placed into two categories, local modes and inter-area modes. Inter-area modes are more difficult to analyze and damp, since they are influenced by global states, and therefore their analysis requires the detail of the inter-connected system.

Local mode oscillations can be greatly improved by a power system stabilizer(PSS),

which acts through the excitation system. But for interarea modes, the damping provided by PSS can be insufficient [15]. Based on the discussion in Chapter 1, we consider an alternative to PSS, a TCSC controller. TCSC can vary the line suscepance quickly and widely, and therefore, TCSC has the potential to improve interarea damping.

Functional sensitivity (also called the residue method) [11] is introduced to study the improvement of damping for a particular mode by the feedback control loop. This method was also used for damping controller design using eigenvalue placement. It was applied to PSS in [12, 13, 14].

When we apply this method to various FACTS devices such as TCSC or SVC, since there are several possible input/output pairs, it would be helpful to obtain a model for control design that is applicable to all of them. Reference [10] provides one. This chapter provides another one which is attractive because of its compact matrix representation.

In this chapter, we first briefly review the fundamental knowledge of small signal stability and linear model of power system. Following that is the introduction to functional sensitivity and control design. Then a unified model of power system for control design is formulated that can be used for various types of control devices at any location. This method is then applied to a TCSC installation in a sample system that has been previously used in the literature.

3.2 Small signal stability

The instability that may result can be of two forms: (i) steadily increasing generator rotor angle due to lack of synchronizing torque, or (ii) rotor oscillations of increasing amplitude due to lack of sufficient damping torque. The latter problem is typically amenable to small signal analysis. Small signal stability is the ability of the power system to maintain synchronism when subjected to small disturbances [16]. A disturbance is considered to be small if the equations that describe the associated dynamics of the power

system may be linearized for the purpose of analysis. Small signal analysis using linear techniques provides valuable information about the inherent dynamic characteristics of the power system and assists in its design.

3.2.1 Eigen properities of linear system

The essential dynamical characteristics of a linear time-invariant system (LTI) of the type

$$\dot{X} = AX + BU \tag{3.1}$$

are expressed in terms of the eigen-properties of the matrix A.

3.2.1.1 Eigenvalues and eigenvectors

The eigenvalues of a matrix A are given by the values of the scalar parameter λ for which there exist non-trivial solutions (i.e., other than $\Phi = 0$) to the equation

$$A\Phi = \lambda\Phi \tag{3.2}$$

where A is an $n \times n$ matrix (real for a physical system such as a power system) and Φ is an $n \times 1$ vector

For any eigenvalue λ_i, the column vector t_i which satisfies Equation (3.2) is called the right eigenvector of A associated with the eigenvalue λ_i. Therefore, we have:

$$At_i = \lambda_i t_i, \qquad i = 1, 2, ..., n \tag{3.3}$$

Similarly, the row vector v_i which satisfies

$$v_i A = \lambda_i v_i, \qquad i = 1, 2, ..., n \tag{3.4}$$

is called left eigenvector of A associated with the eigenvalue λ_i.

3.2.1.2 System modes

In the absence of an input, the state equation of the linear time invariant system assumes the form

$$\dot{X}(t) = AX(t) \tag{3.5}$$

where A is a real $n \times n$ matrix and $X(t)$ is an $n \times 1$ state vector whose variation with time defines the free motion of the system. The precise nature of the free motion of the linear time-invariant system (LTI) following any disturbance can be described in terms of the eigenvalues and eigenvectors of the matrix A.

The equation describing the free motion of the system (3.5) can be expressed in the form

$$X(t) = \sum_{i=1}^{n} t_i[\exp \lambda_i t] v_i X(0) \tag{3.6}$$

Equation(3.6) shows clearly that the free motion of the linear-time invariant system governed by (3.5) is a linear combination of n functions of the form $[\exp \lambda_i t]t_i, (i = 1, 2, ..., n)$ which are said to describe the n dynamical modes of the system. For the power system, we are only concerned about the relative movement of generators. So we always choose one generator as the reference. This results in $n - 1$ relative dynamic modes. Thus, the shape of a mode is described by its associated eigenvector, t_i, and its time-domain characteristics by its associated eigenvalue, λ_i. It is evident from (3.6) that the equilibrium state $X = 0$ of the system (3.5) will be asymptotically stable in the sense that $X(t) \to 0$ as $t \to \infty$ if and only if

$$Re\lambda_i < 0, \qquad i = 1, 2, ..., n \tag{3.7}$$

3.2.1.3 Mode shape

The right eigenvector gives the mode shape, i.e., the relative activity of the state variables when a particular mode is excited. For example, the element t_{ki} of the right

eigenvector t_i gives the degree of activity of the state variable x_k in the ith mode [16].

3.2.2 Lyapunov's first method

The stability in the sense of small signal of a nonlinear system is given by the roots of the characteristic equation of the system of first approximations, i.e., by the eigenvalues of system A matrix [16]:

- When all eigenvalues have negative real parts, the original system is asymptotically stable.
- When at least one of the eigenvalues has a positive real part, the original system is unstable.
- When at least one of the eigenvalues have real parts equal to zero, with all other eigenvalues having negative real parts, then it is not possible on the basis of the first approximation to tell whether the system is stable or unstable.

3.2.3 Power system models

The equations to describe the oscillatory behavior of a power system are composed of a mix of differential and algebraic equations that can be expressed as:

$$\begin{aligned} \dot{X}_1 &= f(X_1, X_2, u) \\ 0 &= g(X_1, X_2, u) \end{aligned} \tag{3.8}$$

where X_1 denotes system state variables, X_2 denotes voltage magnitudes and angles, and u is an output signal for any specific controller of interest. We define y as the controller input so that:

$$y = h(X_1, X_2, u) \tag{3.9}$$

In this research, we use the so called one-axis model of synchronous generators as following:

$$T_{d0i}^{'}\dot{E}_{qi}^{'} = E_{FDi} - E_{qi}^{'} - I_{di}(x_{di} - x_{di}^{'}) \tag{3.10}$$

$$T_{ji}\dot{\omega}_i = M_{Ti} - M_{ei} - D_i * (\omega_i - 1) \tag{3.11}$$

$$\dot{\delta}_i = 2\pi f_0(\omega_i - 1) \tag{3.12}$$

where

ω_i in pu;

δ_i in rad;

$T_{ji} = 2H$ in sec;

$Td0_i^{'}$ in sec;

others in pu.

and a simple exciter model:

$$T_{ai}\dot{E}_{FDi} = -E_{FDi} + K_{ai}(V_{refi} - V_i) \tag{3.13}$$

Such equations constitute the differential equations described in 3.8, where X_1 is corresponding to E_{qi}, ω_i, δ_i and E_{FDi}.

We use the power flow equations as the network equations:

$$\Delta P_i = P_{Gi} - P_{Li} - V_i \sum_{k=1}^{n} V_k(G_{ik}\cos\theta_{ik} + B_{ik}\sin\theta_{ik}) = 0 \tag{3.14}$$

$$\Delta Q_i = Q_{Gi} - Q_{Li} - V_i \sum_{k=1}^{n} V_k(G_{ik}\sin\theta_{ik} - B_{ik}\cos\theta_{ik}) = 0 \tag{3.15}$$

$$(i = 1, 2, ..., n)$$

These network equations are related to the differential equations through the generator terminal conditions. The bus voltage magnitude V_i and angle θ_i, respectively, comprise the vector X_2 used in eqts. 3.8 and 3.9.

By linearization, we obtain:

$$\begin{aligned} \Delta\dot{X} &= A\Delta X + B\Delta u \\ \Delta Y &= C\Delta X + D\Delta u \end{aligned} \tag{3.16}$$

where $\Delta X = \Delta X_1$ is the vector of state variables.

3.2.4 Characteristics of small-signal stability problems

Eigen analysis of the system A-matrix will produce system eigenvalues λ_i and their corresponding right and left eigenvectors t_i, v_i, respectively. Some of the modes are defined as local modes and others are inter-area modes as indicated by the frequency range and system states by which the modes are affected.

3.2.4.1 Local problems

Local problems may be associated with rotor angle oscillations of a single generator or a single plant against the rest of the power system. Such oscillations are called local plant mode oscillations. Local problems may also be associated with oscillations between the rotors of a few generators close to each other. Such oscillations are called inter-machine or inter-plant mode oscillations.

3.2.4.2 Global problems

Global problems are caused by interactions among large groups of generators and have widespread effects. They involve oscillations of a group of generators in one area swinging against a group of generators in another area. Such oscillations are called *inter-area mode oscillations.* Large interconnected systems usually have two distinct forms of inter-area oscillations:

- A very low frequency mode involving all the generators in the system. The system is essentially split into two parts, with generators in one part swinging against

machines in the other part. The frequency of this mode of oscillation is on the order of 0.1 to 0.3 Hz.

- Higher frequency modes involving subgroups of generators swinging against each other. The frequency of these oscillations is typically in the range of 0.4 to 0.7 Hz.

The aim of the design of the controller is to increase the damping of the poorly damped inter-area modes.

3.3 The residue method

3.3.1 Functional sensitivity

Figure 3.1 shows the transfer function of the closed-loop system, where:

$$G(s) = C(sI - A)^{-1}B + D \tag{3.17}$$

is the transfer function of original system, and $KH(s)$ is the transfer function of the controller. K is a constant gain.

The transfer function between the kth input and the jth output $G_{jk}(s)$ can be expressed in terms of residues and system eigenvalues as:

$$G_{jk}(s) = \sum_{i=1}^{n} \frac{R_{ijk}}{(s - \lambda_i)} \tag{3.18}$$

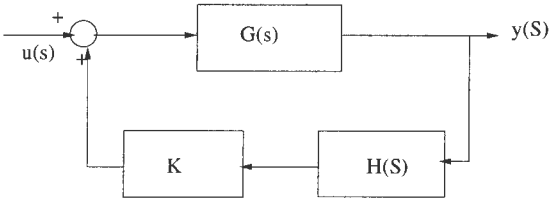

Figure 3.1 Transfer function

where R_{ijk} is the residue associated with ith mode, kth output and jth input. R_{ijk} can be expressed as:

$$R_{ijk} = C_j t_i v_i B_k \tag{3.19}$$

where t_i and v_i denote the right and left eigenvectors, respectively associated with the ith eigenvalue.

Additionally, the residue can be expressed in terms of mode controllability and observability. The controllability of mode i from the jth input is given by:

$$cont_{ij} = |v_i Bj| \tag{3.20}$$

The measure of mode observability of mode i from output k is given by:

$$obsv_{ik} = |C_k t_i| \tag{3.21}$$

It is clear that

$$|R_{ijk}| = |C_k t_i v_i Bj| = obsv_{ik} \cdot cont_{ij} \tag{3.22}$$

Reference [11] shows that the residue associated with an eigenvalue λ_i and a feedback transfer function $\phi(s, K)$, where K is constant gain of the controller, are related by:

$$\frac{\partial \lambda_i}{\partial K} = R_{ijk} \frac{\partial \phi(s, K)}{\partial K} \tag{3.23}$$

Eqt. 3.23 is known as Functional Sensitivity [12]. It gives the relation between the sensitivity of eigenvalue to feedback loop gain and the open loop residue associated with the same eigenvalue.

The feedback transfer function in Figure 3.1 is:

$$\phi(s, K) = KH(s) \tag{3.24}$$

Substitution of $\phi(s, K)$ into eqt. 3.23, and assuming the gain K is small, we have:

$$\frac{\Delta \lambda_i}{\Delta K} = R_{ijk} H(\lambda_i) \tag{3.25}$$

If K=0 in the initial operating point, ΔK is equal to K. Therefore, adding the feedback to the system will cause a change in the ith eigenvalue as:

$$\Delta\lambda_i = R_{ijk} K H(\lambda_i) \tag{3.26}$$

3.3.2 Control design approach

Eqt. 3.26 shows the relation between the change in the ith eigenvalue and residue associated with the ith eigenvalue. For each oscillatory mode, λ_i has a complex conjugate, and so does the corresponding residue. We can design a lead/lag compensation controller to shift the residue to the negative axis, as shown in Figure 3.2, so as to make the real component of $\Delta\lambda_i$ as negative as possible. The form of the compensator design is given in [14] as:

$$KH(s) = K\frac{sT}{1+sT}\left[\frac{1+sT_1}{1+sT_2}\right]^m \tag{3.27}$$

where:

$$\begin{aligned}
\phi &= 180^o - arg(R_{ijk}) \\
\alpha &= \frac{T_2}{T_1} = \frac{1-sin(\frac{\phi}{m})}{1+sin(\frac{\phi}{m})} \\
T_1 &= \frac{1}{\omega_i\sqrt{\alpha}} \\
T_2 &= \alpha T_1
\end{aligned}$$

T is the washout time constant (usually 5-10 sec.), ω_i is the frequency of the poorly damped mode in rad/sec, K is a positive constant gain, and m is the number of compensation stages. The angle compensated by each block should not exceed 60^o.

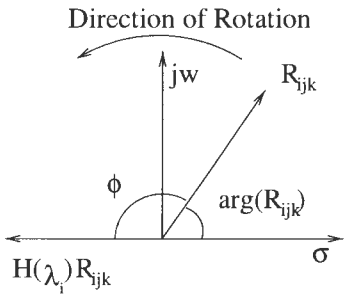

Figure 3.2 Concept of compensation

3.4 General application in power system

In this section we provide an approach for controller design that is generalized in that it can be used for various types of control devices, at any location, by specifying only the controller input and output signal. We assume in this approach that the controller can be modeled in the form given in eqt. 3.27.

3.4.1 Influence of controller output signal

From the concept of residue we know that the controller output signal (i.e., the input signal of the original system) directly affects the controllability and the corresponding residue. Different power system control devices have different output signals. As for PSS, the output of the controller is mixed with V_{ref} as an AVR input; for some of the FACTS devices, the output may be the thyristor firing angle. Representing the controller output signal as u, the linearization of eqt. 3.8 results:

$$\begin{aligned} \Delta\dot{X}_1 &= \frac{\partial f}{\partial X_1}\Delta X_1 + \frac{\partial f}{\partial X_2}\Delta X_2 + \frac{\partial f}{\partial u}\Delta u \\ 0 &= \frac{\partial g}{\partial X_1}\Delta X_1 + \frac{\partial g}{\partial X_2}\Delta X_2 + \frac{\partial g}{\partial u}\Delta u \end{aligned} \tag{3.28}$$

Some manipulation yields:

$$\Delta X_2 = -\frac{\partial g}{\partial X_2}^{-1}\left[\frac{\partial g}{\partial X_1}\Delta X_1 + \frac{\partial g}{\partial u}\Delta u\right] \tag{3.29}$$

$$\begin{aligned}\Delta \dot{X}_1 &= \left[\frac{\partial f}{\partial X_1} - \frac{\partial f}{\partial X_2}\frac{\partial g}{\partial X_2}^{-1}\frac{\partial g}{\partial X_1}\right]\Delta X_1 \\ &+ \left[\frac{\partial f}{\partial u} - \frac{\partial f}{\partial X_2}\frac{\partial g}{\partial X_2}^{-1}\frac{\partial g}{\partial u}\right]\Delta u\end{aligned} \tag{3.30}$$

Comparison of eqt. 3.29 to eqt. 3.16 indicates that the matrix A and vector B in eqt. 3.16 are:

$$A = \frac{\partial f}{\partial X_1} - \frac{\partial f}{\partial X_2}\frac{\partial g}{\partial X_2}^{-1}\frac{\partial g}{\partial X_1} \tag{3.31}$$

$$B = \frac{\partial f}{\partial u} - \frac{\partial f}{\partial X_2}\frac{\partial g}{\partial X_2}^{-1}\frac{\partial g}{\partial u} \tag{3.32}$$

Eqt. 3.31 and 3.32 show that different choice of the controller output signal u only affects the B vector, and it has no influence on A matrix.

3.4.2 Influence of controller input signal

The controller input signal is related to the residue via the observability. Generator frequency deviation, bus voltage and real power flow are all good candidates for controller local input signals. If one is willing to accept additional expense associated with communication, global signals such as intermachine speed difference may be used. Representing these kinds of signals, global or local, as y, the linearization of the output signal in eqt. 3.16 yields:

$$\Delta y = \frac{\partial h}{\partial X_1}\Delta X_1 + \frac{\partial h}{\partial X_2}\Delta X_2 + \frac{\partial h}{\partial u}\Delta u \tag{3.33}$$

Substitution of eqt. 3.29 results in:

$$\begin{aligned}\Delta y &= \left[\frac{\partial h}{\partial X_1} - \frac{\partial h}{\partial X_2}\frac{\partial g}{\partial X_2}^{-1}\frac{\partial g}{\partial X_1}\right]\Delta X_1 \\ &+ \left[\frac{\partial h}{\partial u} - \frac{\partial h}{\partial X_2}\frac{\partial g}{\partial X_2}^{-1}\frac{\partial g}{\partial u}\right]\Delta u\end{aligned} \tag{3.34}$$

Comparison to eqt 3.16 indicates that:

$$C = \frac{\partial h}{\partial X_1} - \frac{\partial h}{\partial X_2}\frac{\partial g}{\partial X_2}^{-1}\frac{\partial g}{\partial X_1} \tag{3.35}$$

$$D = \frac{\partial h}{\partial u} - \frac{\partial h}{\partial X_2}\frac{\partial g}{\partial X_2}^{-1}\frac{\partial g}{\partial u} \tag{3.36}$$

Therefore, different controller input signals result in different C and D vectors.

3.4.3 Determination of controller gain

The controller gain K is computed as a function of the desired eigenvalue location $\lambda_{i,des}$ according to eqt. 3.26 so that:

$$K = \frac{\lambda_{i,des} - \lambda_i}{R_{ijk}H(\lambda_i)} \tag{3.37}$$

where we assume that the phase compensation of $H(\lambda_i)$ provides that K is real. Since eqt. 3.26 is derived under the assumption that K is small, the eigenvalue after the controller design may be different from the desired one. Moreover, we need to check that the influence of the controller on the other modes is acceptable; if not, or under the condition that we desire to damp more that one mode, we may replace R_{ijk} in eqt. 3.27 and eqt. 3.37 with a weighted summation of the residue for all modes. This approach for damping multiple modes may require several interations.

3.4.4 Location problem

From eqt. 3.26, it is easy to see that for the same gain of the feedback loop, a larger residue will result in a larger change in the corresponding mode. Therefore the best input and output of the controller are those which give the largest residue for the desired mode. Reference [24] addresses the problem of TCSC location from this perspective.

One practical consideration in choosing the input/output pair is the cost of the compensator. Therefore, high residue input/output pairs that require more that 60^o

phase shift may be less desirable than lower residue pairs that require less that 60^o of phase shift, since 60^o is an approximate phase limit for each compensator stage.

3.5 Application to TCSC

3.5.1 Calculation of system matrix of controller output

The design method mentioned above is suitable for application to any controller. Here, we apply it to TCSC. We assume that the impedance associated with the TCSC is:

$$x_{TCSC} = x^{(0)}_{TCSC} + \Delta x_{TCSC}(s) \tag{3.38}$$

$$\Delta x_{TCSC}(s) = \frac{\Delta x T_{TCSC}}{1 + sT_{TCSC}} \tag{3.39}$$

where $x^{(0)}_{TCSC}$ is the steady state impedance of the device and $\Delta x_{TCSC}(s)$ represents the control influence on the TCSC impedance. T_{TCSC} is the time constant of TCSC which is 0.015s, and ΔZ is the module signal from the controller [25]. So the line impedance after installation of TCSC is:

$$Z_{line} = Z^{(0)}_{line} - jx_{TCSC} \tag{3.40}$$

where $Z^{(0)}_{line}$ is the line reactance in steady state. Since the reactance of the line is constant, the change in total line reactance is:

$$\Delta Z_{line} = -j\Delta x_{TCSC}(s) \tag{3.41}$$

Hence we can take the change of impedance of a transmission line as the output of the controller. By substituting Z_{line} for u in eqt. 3.32, the B matrix can be calculated. The TCSC control loop is shown in Fig. 3.3.

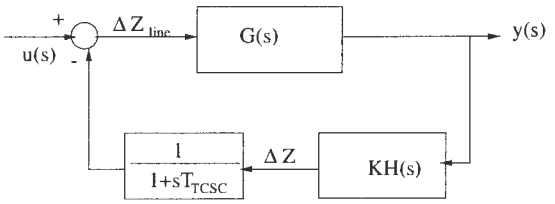

Figure 3.3 Controller loop of TCSC

3.5.2 Influence of different controller input

TCSC is more effective in damping interarea oscillations when the controller input is a global signal. We have found that the speed difference of two generators which oscillate against each other gives a large observability, and so does the change in tie line real power flow. So either of these signals can serve as the input to TCSC controller.

Using speed difference as the controller input signal, since the changes of speed are state variables, the output Y can be expressed as:

$$\Delta Y = a\Delta X_1 \tag{3.42}$$

where: $a = [0, 0, \cdots, 0, 1, \cdots, -1, 0, \cdots, 0]$ and 1 and -1 in the a vector corresponds to the speed difference as $\Delta\omega_i - \Delta\omega_j$. Therefore from eqt. 3.35 the C and D matrices are: $C = a$ and $D = 0$.

Interarea modes typically have high observability in the active power of tie lines between areas involved in the interarea oscillation and high controllability in the susceptance of the same line. So it is efficient and practical to install TCSC in a tie line and use the line active power flow as the controller input.

The tie line active power flow is a function of voltage magnitude and angle, which comprise X_2. Therefore we may write:

$$P = h(X_2) \tag{3.43}$$

By setting $\frac{\partial h}{\partial X_1} = 0$ in eqt. 3.35, C and D can be easily computed.

3.5.3 Determination of location

When a TCSC is installed in a system, it can be considered as fixed compensation (corresponding to the TCSC reference signal) under steady state conditions and controlled compensation under transient or oscillatory conditions [26]. Therefore, the determination of the location of TCSC should involve two major steps. First, determine the location of TCSC assuming it is simply fixed compensation. This is equivalent to siting a conventional series capacitor, a problem which also needs to account for other factors besides modal behavior such as active/reactive line flow and voltage control. Second, determine the best location for siting controlled compensation. This can be done using functional sensitivity analysis. This two step method is developed in [24].

In order to compare the residue associated with different input and output signals, we form the $\hat{B}$ and $\hat{C}$ matrices. These two matrices are related to the B and C vector in eqt. 3.32 and eqt. 3.35. The kth column of the $\hat{B}$ matrix is a specific B vector and denotes the influence of change in susceptance of the kth line on the system state. The jth row in the $\hat{C}$ matrix is a specific C vector and represents one possible combination of speed difference when the input to the controller is the speed difference signal; for the input of tie line flow, the jth row represents the line number from which the power flow signal comes. Then, the residue matrix can be calculated as:

$$R_i = \hat{C} t_i v_i \hat{B} \tag{3.44}$$

The k and j associated with the location in R_i of the largest residue gives the best location and controller input signal.

If the controller uses only local measurements, the input and output are associated with the same circuit. Therefore, consideration of local signals requires that we choose the largest element on the diagonal of the residue matrix in eqt. 3.44.

Note that the line associated with the largest residue for speed difference input signal may not be the same as the line associated with the largest residue for tie line flow input

signal. This is because for each line the observability factor for speed difference is not the same as the observability factor for tie line flow. In addition, we note that when using a speed difference input signal, since there is no local measurement of such a signal, we choose the machine speed differences that give the largest observability, and we use the same speed difference signal for all lines considered as potential locations. Therefore in the case of speed difference signal, the observability factor is the same for all candidate locations, and the TCSC effectiveness depends only on controllability. On the other hand, when using the tie line real power flow as TCSC input, a local measurement, the input is unique to each candidate location, and the effectiveness depends on both controllability and observability of the same line.

3.5.4 Numerical example

A 3-area, 6-machine sample system [22] presented in Figure 3.4 is used to illustrate the siting and control approach. This system gives 3 local modes and 2 interarea modes. Although this is a test system, it well serves to illustrate the approach, which remains the same for large systems. The upperline between 10-11 is an equivalent line [22] with impedance smaller than the lower one. So it is not an candidate for compensation. These two lines serves as a tie line that connects area A with the others, so the lower line is a good candidate to install TCSC, as confirmed by the procedure given in reference [24]. The TCSC's fixed compensation level is set to 40%. Stressing the system by increasing the load at bus #10 and generation at bus #6, one interarea oscillatory mode becomes unstable, as indicated in Table 3.1.

The mode shape of the generator speed ω deviation for the unstable mode is shown in Figure 3.5. It clearly shows that the group of generators 3 and 4 oscillate against the group of generators 5 and 6.

In Table 3.3, we compare the residue of the two interarea modes for the input/output pairs of Table 3.2. The phase of mode 1 and 2 are close for each controller input; also it

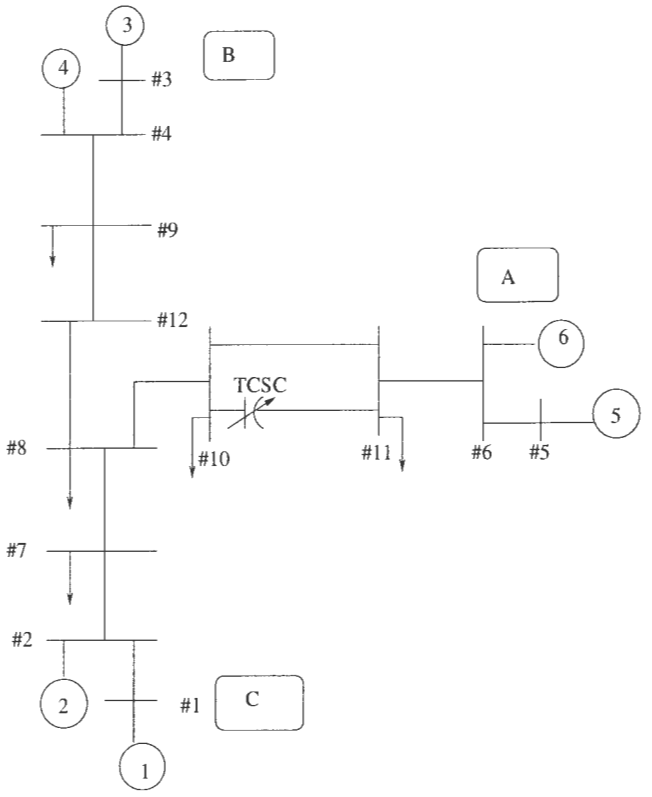

Figure 3.4 Sample system

is shown in Table 3.1 that the frequency of these two interarea modes are close to each other. Therefore, a controller designed using either of these two modes will also improve the other. Since mode 1 is unstable, we will use the residue and frequency of mode 1 for the controller design.

Setting the desired damping ratio ξ for mode 1 as 20 %, we use eqt. 3.37 to calculate the gain K. The two interarea modes are shown in Table 3.4, where the load at bus #10

Table 3.1 Interarea modes

Real Load at Bus #10		100 MW	500 MW
Mode 1	f(Hz)	0.9039	0.8882
	ξ%	1.8278	-0.2475
Mode 2	f(Hz)	1.1527	1.1349
	ξ%	7.9025	6.8664

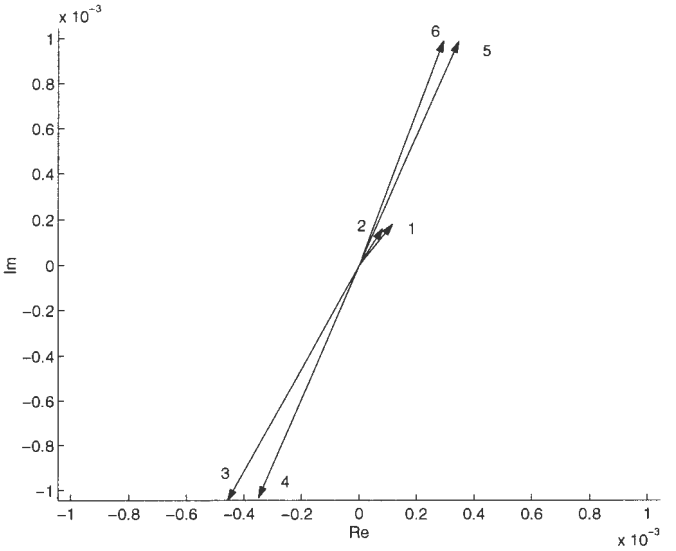

Figure 3.5 Mode shape of mode 1

Table 3.2 Residues of different controller input

	Speed diff.	Tie line flow
$Residue_{max}$	0.1537	0.3342
Input Signal	$\Delta\omega_4 - \Delta\omega_6$	$\Delta P_{tie10-11}$
Location	Line 10-11	Line 10-11

is 500 MW. For the same mode 1 damping ratio, the controller using tie line flow signal has smaller feedback gain. The difference between desired and calculated damping ratio is due to the fact eqt. 3.26 is exact only for very small feedback gain, which we verified through calculation. In addition, we observe that the other interarea mode (mode 2) has not been degraded significantly by either controller. Table 3.5 also indicates no significant degradation occurs in the local modes as well.

The performance of the controller can also be shown in terms of the increase of transfer capacity. Without TCSC, the maximum load at bus #10 is 400 MW. When TCSC with the controller using speed difference as the input is installed, the maximum load is 550 MW. When TCSC with the controller using tie line real power flow is installed,

Table 3.3 Residues of two interarea modes

	Speed diff.		Tie line flow	
	Mode1	Mode2	Mode1	Mode2
Residue	0.1537	0.0286	0.3342	0.3342
Phase(Residue)	20.258	51.129	89.756	67.771

Table 3.4 Damped modes

Feedback loop gain $K \times \lvert H(\lambda_i)\rvert$	Original		Tie line flow 3.4646		Speed diff. 7.3343	
	$f(Hz)$	$\xi\%$	$f(Hz)$	$\xi\%$	$f(Hz)$	$\xi\%$
Mode 1	0.8882	-0.2475	0.8593	45.1690	0.8224	19.9201
Mode 2	1.1349	6.8664	0.9688	9.1942	1.1027	9.7090

the maximum load is 800 MW, which is twice that of the load without TCSC. Therefore, the TCSC controller yields an expanded secure operating region, and we find that use of tie line flow input signal is more effective than use of speed difference input signal.

3.6 Conclusions

This chapter presents the unified power system model for control design. Combined with residue method that it can be used to design various kinds of power system controllers. The method is illustrated by applying it to TCSC controller design for damping

Table 3.5 Other modes

Mode	Original		Tie line flow		Speed diff.	
	$f(Hz)$	$\xi\%$	$f(Hz)$	$\xi\%$	$f(Hz)$	$\xi\%$
A	1.8553	4.4060	1.8613	5.8725	1.8565	4.8270
B	1.7186	5.4928	1.7188	4.7851	1.7174	5.7120
C	1.6840	6.0635	1.6839	5.9582	1.6841	6.0898

interarea oscillations. This method also results in selection of the best location and input signal for TCSC. A numerical example illustrates the effectiveness of TCSC damping performance. Also it shows that for this test system, the tie line flow signal is more effective than speed difference signal as the input of TCSC. Use of tie line flow rather than speed difference as TCSC input signal is attractive since it is based on local measurements only.

This method is straightforward and easy to apply. It has been successfully used in PSS because influence of PSS is limited. On the other hand, TCSC can significantly affect many modes. We shall see in next chapter that this fact create a greater concern for controller robustness when using a TCSC controller.

CHAPTER 4 DEMAND FOR THE ROBUST CONTROLLER

4.1 Introduction

The residue control design method mentioned in last chapter works very well for the sample system. The major problem of this method is that it uses the linearized system at particular operating point. It does not take into account the uncertainties in that operating point. Moreover, this method is designed to control one mode. Although we can use some weighting function to consider more modes, the performance of the controller for all these modes are not guaranteed under different set of system parameters. TCSC has potential large global influence on the modes since it is a transmission line impedance controller and consequently can easily influence the dynamic of the entire system. This is not the case with traditional PSS controller because PSS affects the system only through one generator. Is there potential for using the residue control design method for TCSC design to improve one or two modes under one operating condition while degrading other modes, or, under other operating conditions, has bad performance or even degrading any other modes?

Paper [15] compared the modal controllability between three kinds of FACTS device and PSS. It analytically shows that the direct contribution of the FACTS-based stabilizer is through all the generators in the power system, while that of PSS is merely through the generator where it is installed. It is consistent with our concern that the FACTS based stabilizer has poor robustness against the changes in power system configuration

and operating condition.

There are many uncertainties in power system models, such as variation of operating point and measurement errors. It is known that data characterizing the load for dynamic studies is hard to obtain by measurement, but that it is very influential on study results. Therefore, in this chapter, we study the impact of load modeling on TCSC and PSS influence of system modal behavior. Instead of comparing only modal controllability [15], we use the functional sensitivity as the criteria, which include modal controllability and observability, because the input, which determines the modal observability, also has great influence on the controller's performance. Like in Chapter 3, the performance of the controller using tie line real power flow as the input, is different from the one using the difference of speed deviation of generators as the input.

4.2 Modeling PSS for residue method

In order to calculate the transfer function of PSS, we need to determine first the input and output signal of the controller, i.e., the u and y in Fig. 3.1.

The output of PSS can be considered as the change of V_{ref}, and the input to PSS is the generator speed deviation $\Delta\omega$. Therefore, $u = \Delta V_{refi}$ and $y = \Delta\omega_i$ when the PSS is installed in the ith generator. Denotes f_{ij} where $(j = 1, 2, 3, 4)$ from equations 3.13, 3.11, 3.12, 3.12 for the ith generator as:

$$\begin{aligned} \dot{E}_{FDi} &= f_{i1}(X_1, X_2, u) \\ \dot{E}'_{qi} &= f_{i2}(X_1, X_2, u) \\ \dot{\omega}_i &= f_{i3}(X_1, X_2, u) \\ \dot{\delta}_i &= f_{i4}(X_1, X_2, u) \end{aligned} \tag{4.1}$$

where

$$\begin{aligned} X_1 &= [E_{FD1}, E_{q1}, \omega_1, \delta_1, \cdots, E_{FD1}, E_{q1}, \omega_1, \delta_1, \cdots]' \\ X_2 &= [V_1, \theta_1, \cdots, V_1, \theta_1, \cdots]' \end{aligned} \tag{4.2}$$

Then for the choice of variables and equations as above, the state space representation is:

$$\begin{aligned} \frac{\partial f}{\partial u} &= [0, 0, \cdots, 0, K_{ai}/T_{ai}, 0, \cdots, 0, 0]^T \\ \frac{\partial g_i}{\partial u} &= 0vector \end{aligned} \tag{4.3}$$

where g is the network equation defined in eqt. 3.14, $0vector$ indicates a vector of 0s. K_{ai}/T_{ai} corresponds to $\frac{\partial f_{i1}}{\partial u}$ and

$$\begin{aligned} \frac{\partial y}{\partial X_1} &= [0, 0, \cdots, 1, 0, \cdots, 0] \\ \frac{\partial y}{\partial X_2} &= 0vector \\ \frac{\partial y}{\partial u} &= 0vector \end{aligned}$$

where 1 corresponds to $\partial y/\partial \omega_i$. Other partial differentials are the same as TCSC. Then the A, D matrices and B, C vectors can be determined from eqts. 3.31, 3.32, and 3.35.

4.3 Comparison of residue between PSS and TCSC

We use the same sample system as for the previous chapter. In this case, the load at bus #10 is increased to 600MW. Also, the load representation is set to 50% constant impedance and 50% constant current, instead of 100 % constant impedance as in chapter 3. This kind of load composition is very commonly used for stability study in case accurate load data is not available [16]. For this data, the modes are listed in Table 4.1, where mode A, B and C are local modes and mode 1 and 2 are interarea modes. and corresponding mode shapes are shown in Fig 4.1 4.2 4.3 4.4 4.5.

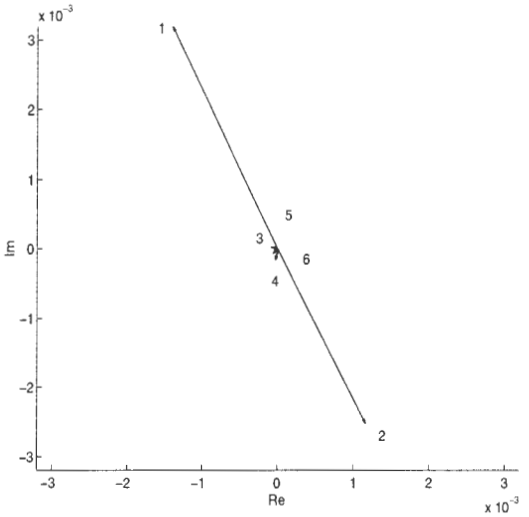

Figure 4.1 Modeshape of mode A

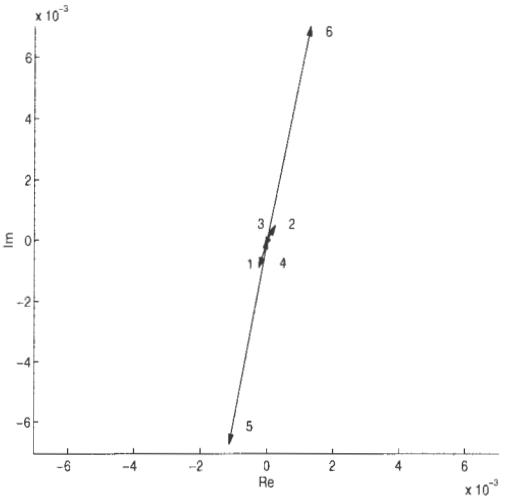

Figure 4.2 Modeshape of mode B

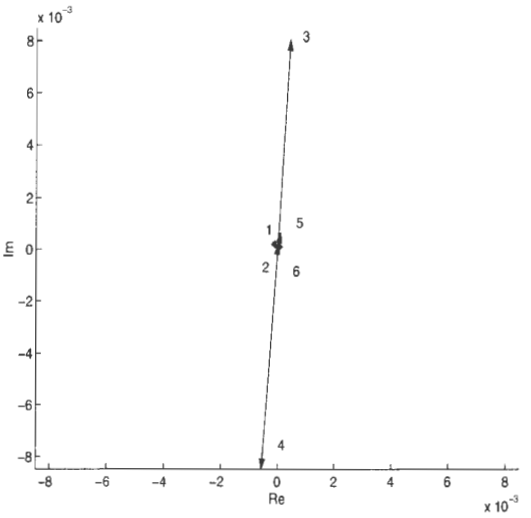

Figure 4.3 Modeshape of mode C

Table 4.1 Modes

Mode	$f(Hz)$	$\xi(\%)$
A	1.8636	4.2955
B	1.7491	5.4896
C	1.6850	6.0390
1	1.0951	5.4225
2	0.8856	-0.9510

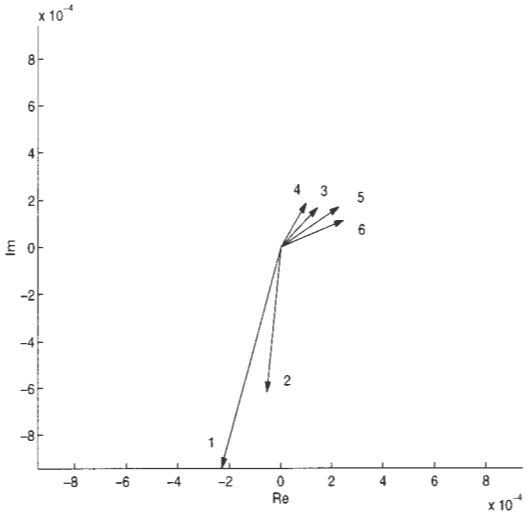

Figure 4.4 Modeshape of mode 1

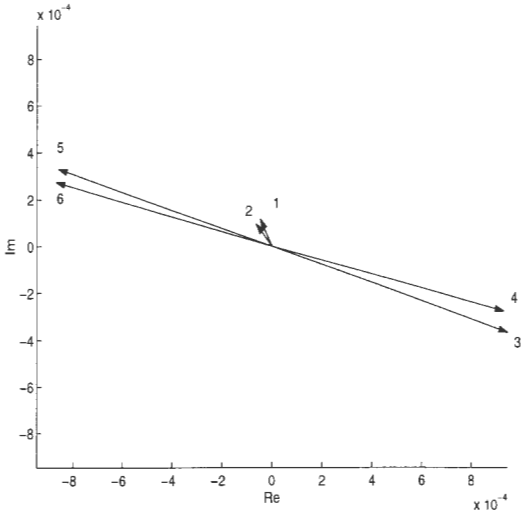

Figure 4.5 Modeshape of mode 2

The modal functional sensitivity of PSS in each generator and TCSC for line 10-11 are listed in Table 4.2. Here TCSC uses tie line real power flow as the input signal. Comparison of modes shapes and the modal functional sensitivities of the PSS indicates that they are closely related. For example, generator #1 participates in local mode A and mode 1, therefore, the corresponding functional sensitivities in these modes are relatively high. However, generator #1 has low residue in all other modes. But for TCSC, that is not the case, i.e., it has relatively high residue for most of the modes. This is because TCSC is acting on the system through all the generators and not just one as for PSS.

Table 4.2 Modal functional sensitivity

		Modes				
	Gen.	A	B	C	1	2
P S S	1	0.06658	0.00085	0.00028	0.06968	0.00037
	2	0.07071	0.00024	0.00004	0.03029	0.00052
	3	0.00005	0.00000	0.08727	0.00680	0.02308
	4	0.00018	0.00002	0.08395	0.00619	0.02339
	5	0.00015	0.09096	0.00007	0.01098	0.02168
	6	0.00015	0.07710	0.00001	0.01106	0.02343
TCSC		0.01525	0.00432	0.00031	0.28580	0.40574

Table 4.2 also shows that PSS has very low influence on the two interarea modes, which are designated as mode 1 and 2. Gens. #3 and #4 oscillate against the group of Gens. #4 and #5. But the corresponding functional sensitivities are only 1/20 of those for TCSC. On the other hand, the fact that TCSC has low impact on local modes indicates it does not have significant local control potential.

Notice that the functional sensitivity of TCSC for both of the two interarea modes are quite similar. Therefore, controller design for one interarea mode must also account for the influence on the other. Using linear system based design, this coordination problem can be difficult for a single operating condition. It is very awkward when the operating conditions change or when there are large uncertainties in system parameters (e.g., uncertainties in load composition) because we can not guarantee that one or more modes will not be degraded and possibly destabilized. This will be illustrated in the following section.

4.4 Robustness of TCSC and PSS

In this section, we use the residue method to design the controller of TCSC and PSS under a given load model. Then we compare the damping influence of these controllers

for different load models.

4.4.1 Load modeling

A static load model expresses the characteristics of the load at any instant of time as algebraic functions of bus voltage magnitude and frequency at that instant. The active power component P and the reactive power component Q are considered separately. The polynomial form of the load modeling follows [16]:

$$\begin{aligned} P_{Li} &= P_{Li0}[p_1(\frac{V_i}{V_{i0}})^2 + p_2(\frac{V_i}{V_{i0}}) + p_3](1 + p_f\Delta f) \\ Q_{Li} &= Q_{Li0}[q_1(\frac{V_i}{V_{i0}})^2 + q_2(\frac{V_i}{V_{i0}}) + q_3](1 + q_f\Delta f) \end{aligned}$$

The coefficient of these static load characteristics can be obtained from two approaches: one is measurement based and the other is components based. For the measurement based approach, the load characteristics are measured at representative substations and feeders at selected times of the day and season. Then these measurements are used to estimate the parameters of the load throughout the system. For the components based approach, the parameters are calculated from billing data [27]. Therefore, these parameters are low in accuracy. In contrast to this low accuracy, these parameters have great influence on system dynamic behavior.

In the analysis of small signal stability, we assume the frequency at buses remain at the rated value, so we eliminate the terms related to frequency.

4.4.2 Comparison of damping performance

The controllers for PSS and TCSC are designed using a load model of 50% constant impedance and 50% constant current. This load model is commonly used for industry stability studies. Based on the comparison of residues in the previous section, TCSC is installed in line #11 to #13 and the active power flow of line is used as the TCSC input. PSS is installed in Gen. #6 and local speed deviation is used as the input.

The desired damping ratios are set to 20% for mode 1 for both PSS and TCSC. The input/output pair is chosen as the method described in chapter 3, so that the controller will improve both interarea modes. The damping results for the designated condition are listed in Table 4.3. From the damping results in Table 4.3 we notice that although the controller loop gain for PSS is much higher than TCSC, the resulting damping ratio is still much smaller than that of TCSC. This implies that TCSC is more effective in damping interarea oscillations.

Table 4.3 Damped modes

Feedback loop gain $K \times \lvert H(\lambda_i)\rvert$	Original		PSS		TCSC	
			50.74		2.940	
	$f(Hz)$	$\xi\%$	$f(Hz)$	$\xi\%$	$f(Hz)$	$\xi\%$
Mode 1	0.8856	-0.9514	0.8945	9.2078	0.8822	41.8090
Mode 2	1.0951	5.4225	1.1202	9.1779	0.9625	8.3966

The performance for the same controller under different load representation is listed in Tables 4.4 and 4.5. It is shown in Tables 4.4 and 4.5 that TCSC can preserve a relatively large damping ratio for the designated mode (mode 1) under different load representation. But because TCSC has great influence on the other modes, the performance of the other mode decreases from 10.9% to -0.355%. For PSS, one the other hand, PSS has a 'flat' performance for the changes in load model. Although it can not provide a high damping ratio for designated modes as TCSC can, it does not degrade the other modes much either. Therefore, use of TCSC as a controller requires that the designer emphasize design robustness much more relative to typical PSS design.

Another interesting phenomenon is the trend of damping ration vs. the changes of load model. When the load composition changes from 100% constant impedance to 100% constant power, it does not necessarily degenerate the system. By the calculation in some small signal stability programs (e.g., MASS), we notice that weather or not the

Table 4.4 Controller performance for interarea modes under different load modeling (Mode 1)

Load Models			Original		PSS		TCSC	
Z	I	P	$f(Hz)$	$\xi\%$	$f(Hz)$	$\xi\%$	$f(Hz)$	$\xi\%$
100	0	0	0.8745	1.2493	0.8790	10.0000	0.9325	38.8750
50	50	0	0.8856	-0.9510	0.8945	9.2078	0.8822	41.8090
50	0	50	0.8974	-0.6560	0.9125	8.3320	0.8414	43.1570
0	50	50	0.9111	-0.2820	0.9391	7.2391	0.8125	43.1590
0	0	100	0.9243	0.6522	0.9738	11.0400	0.7959	42.0960

Table 4.5 Controller performance for interarea modes under different load modeling (Mode 2)

Load Models			Original		PSS		TCSC	
Z	I	P	$f(Hz)$	$\xi\%$	$f(Hz)$	$\xi\%$	$f(Hz)$	$\xi\%$
100	0	0	1.1212	6.7240	1.1456	9.4103	0.9553	10.9090
50	50	0	1.0951	5.4225	1.1202	9.1779	0.9625	8.3966
50	0	50	1.0648	3.2133	1.0875	8.6354	0.9653	5.8797
0	50	50	1.0305	-0.5130	1.0401	7.6175	0.9648	3.1007
0	0	100	0.9972	-0.7020	0.9775	0.4722	0.9615	-0.3550

change of load composition from 100% constant impedance to 100% constant power at one load bus will degenerate the system depends on the location of that load. For a multi-machine system, the influence of changes in load composition at each load bus will be different. Therefore, when we change the load composition at all the buses, the trend of system damping ration is not determinant.

4.5 Conclusion

In this chapter, the functional sensitivities of PSS and TCSC are compared. It is shown that TCSC has much larger residue for the interarea mode than PSS. Then we compare the performance of TCSC and PSS controller under different load representa-

tion. We find that TCSC has very large damping ratio for the designated mode, but poor performance for the other mode under other sets of load parameters.

There are several way to deal with the controller performance under different operating conditions, with the consideration of several the modes. We can design a set of controller parameters for different situations, which is a kind of adaptive control. But as mentioned in Chapter 1, the operating condition of power system changes quickly and dramatically. This approach would require a large amount of controller data.

Another way is to tune the controller data so that the control parameter provides the maximum possible improvement in one or mode modes without significantly degrading other modes. However, this approach require tedious iterations and the result can not be guaranteed under all conditions.

In next chapter, we attempt to use the newly developed μ analysis and synthesis method to study the TCSC behavior. This method is promising with respect to a controller design with the consideration of uncertainties.

CHAPTER 5 μ ANALYSIS AND SYNTHESIS FOR THE UNCERTAINTIES IN STATIC LOAD MODELING

5.1 Introduction

In the last chapter, we compared the performance of TCSC and PSS under different load representation. It is shown that TCSC has more global influence on the system stability. When we have more than one mode need to be considered, TCSC designed under one operating condition can have poor performance on other modes under different conditions.

The idea of robust control is developed to deal with such situations. It takes into account all the modes ith the modeling error at the time of controller design using what is called uncertainty modeling. Such uncertainty models can be put into two categories, one is structured uncertainties, for which the uncertainty matrix is diagonalized. The other is unstructured uncertainties, which does not have such structure. As shown in Fig. 5.1, when the Δ block can be diagonalized, we call the uncertainties as structured uncertainties and vice versa.

Most work related to robust control applications in power systems deal with the unstructured uncertainties [19, 20, 21]. These approaches are easy to apply but conservative. Papers [22, 23] formulates the uncertainties into structure. Uncertainties act on the plant model either linearly or nonlinearly. The μ approach is designed to deal with uncertainties which have linear impact on the system. If we try to use μ on uncertainties that act on the plant nonlinearly, it requires additional linearization or approximation

to make the problem suitable for the μ analysis. This may result in low accuracy.

From last chapter we know that the load model plays an important role in system stability, and an accurate load model is hard to obtain. Our goal is to model the uncertainties in static load modeling using structured uncertainties. Then we will use the μ analysis and synthesis to design a controller that may damp the system in a large range of load composition.

We first give a brief introduction to the basic concepts of robust control and uncertainties. Then we model the uncertainties in load representation. Our study shows that such uncertainties act on the plant model linearly. Then we use the structured singular value analysis, i.e. the μ analysis to study the system behavior for such kinds of uncertainties, and we test the correctness of the uncertainty modeling. A robust controller is designed using μ synthesis, and the damping performance is compared with the controller designed by residue method.

5.2 Fundamentals

5.2.1 Plant uncertainty

Figure 5.1 shows a conventional closed loop system. Controller K is usually designed to work with a single nominal plant model $G = G_{nom}$. But G_{nom} never matches the true plant's behavior. The actual plant can be written as $G_{act} = G_{nom} + \Delta$, where Δ is simply the difference between the nominal plant and the actual plant. A real-world controller must work properly for all operators Δ in some set.

5.2.2 Small gain theorem

In order to study the impact of these uncertainties on the system behavior, we introduce the small gain theorem, which is a fundamental idea in robust control. First we need to define the normed space, transfer function norm, and infinite norm.

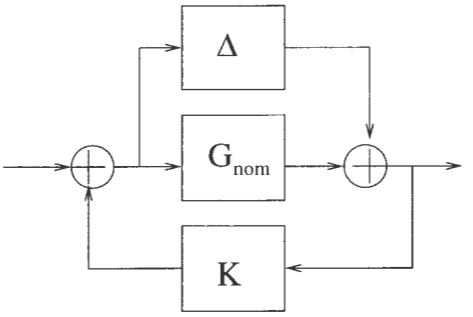

Figure 5.1 Plant model

5.2.2.1 Norm of transfer function

Any transfer function matrix $G(x)$ and its impulse response $g(t)$ can be considered as a matrix-valued signal or time function. As with a scalar signal, or a scalar function of a continuous time variable, a transfer function have a 1-norm, a 2-norm and a ∞ - norm that are defined in a manner analogous to the corresponding vector norms. The set of all possible signals that have finite values for these norms form normed spaces (Banach spaces).

H_∞ is the space we define the infinity norm, which is defined as functions $F(s) \in C^{m*n}$ analytic in $Re(s) > 0$ (no right hand side pole) which satisfy:

$$\bar{\sigma}(F(s)) < \infty \tag{5.1}$$

for any $Re(s) > 0$. Where $\bar{\sigma}$ is the upper bound of the singular value of function $F(s)$ evaluated at each $s \in C^{m*n}$.

The H_∞ is a stable space, since all the functions in this space do not have right hand side pole. Moreover, its domain is over the entire complex plane (i.e., for all the possible value of s). So it is the space of transfer function, not just frequency response in some particular frequency. The transfer function infinite norm is given by:

$$\| G(s) \|_\infty = \sup_{\omega \in R} \bar{\sigma}(G(j\omega)) \tag{5.2}$$

5.2.2.2 Small gain theorem

Assume that $G_1, G_2 \in H_\infty$ are both stable, bounded gain transfer functions. Then if $\| G_1G_2 \|_\infty < 1$, the closed-loop system is stable. Furthermore, since $\| G_1G_2 \|_\infty \leq \| G_1 \|_\infty \| G_2 \|_\infty$, then:

$$\| G_1 \|_\infty \| G_2 \|_\infty < 1 \tag{5.3}$$

guarantees the closed-loop stability.

The norm used in small gain theorem may be also addressed in other normed space, but the infinite norm can give some nice result. According to the definition of infinite norm in eqt. 5.2, the small gain theorem can be extended to singular value analysis. For the perturbation Δ in Fig. 5.2, the perturbed system is stable if:

$$\bar{\sigma}(\Delta)\bar{\sigma}(M) < 1 \tag{5.4}$$

for all frequencies ω where $\Delta(s)$ and $M(s)$ are evaluate on imaginary axis $s = j\omega$.

5.2.3 The Structured singular value

5.2.3.1 Definition

Let $\Delta = diag(\Delta_1, \Delta_2, \cdots, \Delta_n)$ be a block diagonal matrix. Let B_Δ denote the set of all Δ matrices with a given, fixed block diagonal structure. The individual Δ_i block may be either scalar or matrix. Assume that $\Delta_i \in C^{k_i \times k_i}$; that is, each Δ_i is a square $k_i \times k_i$ complex matrix.

The block diagram of Fig 5.1 can be transformed into that of Fig. 5.2. Therefore, the structural singular value of matrix M, denoted $\mu(M)$, is defined as:

$$\frac{1}{\mu(M)} = \inf_{\Delta \in B_\Delta} \{\bar{\sigma}(\Delta) s.t. \det(I - \Delta M) = 0\} \tag{5.5}$$

where $\bar{\sigma}$ is the maximum singular value. If no $\Delta \in B_\Delta$ exist to satisfy $\det(I - \Delta M) = 0$, let $\mu(M) = 0$. So $\frac{1}{\mu(M)}$ is the size of the smallest "destablizing" $\Delta \in B_\Delta$, since

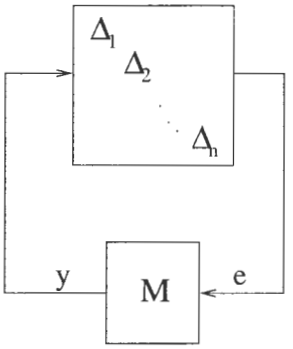

Figure 5.2 Structure singular value

$\det(I - \Delta M) = 0$ determines the stability boundary of the closed loop system, in which situation at least one zero eigenvalue appears. The computational effort of μ has been well illustrated in [18].

5.2.3.2 Properties of μ

There are several properties of μ which are very useful for studying stability of a system. Define:

$D = diag(d_1 I_{k1}, d_2 I_{k2}, \cdots, d_n I_{kn})$ where $d_i \in R, d_i > 0, I_{ki}$ is a identity matrix.

$U = diag(U_1, U_2, \cdots, U_n), s.t. U_i \in C^{k_i * k_i}, U_i^* U_i = I_{ki}$

Where *diag* means a diagonal matrix with the diagonal elements as in the parenthesis. Then we have two important properties of μ which will help us in the stability analysis and control design:

$$\begin{aligned} D\Delta D^{-1} &= \Delta \qquad (5.6) \\ \max \rho(UM) &\leq \mu(M) \leq \inf \bar{\sigma}(DMD^{-1}) \end{aligned}$$

where $\rho(UM)$ is the spectrum radius of UM.

When the number of uncertainties is less than 3, the second 'less than or equal to' in the second inequality relation of eqt. 5.6 can be changed to 'equal to'. Unfortunately, for most of the situations, the number of uncertainties is larger than 3. So we can not obtain

the value of μ, instead, we can only bound μ from above and below. By the calculation of the bounds of μ, i.e. the μ analysis, we can determine the worst-case effect on stability or performance when several parameters of a controlled plant vary simultaneously. This will also help us to design the controller whose performance is guaranteed under such uncertainties.

5.2.4 Assessing robust stability with μ analysis

From the definition of μ and the small gain theorem, we have: $\mu(M)\mu(\Delta) < 1$ guarantees the closed-loop stability. Note for a block diagonal $\Delta \in B_\Delta$, $\bar{\sigma} = \max \bar{\sigma}(\Delta_i)$. That is, the overall gain of Δ is equal to the gain of its largest diagonal block. Therefore, if we know the maximum gain of Δ, we can compute the range of μ , such that if

$$\frac{1}{\mu(M)} > \bar{\sigma}(\Delta) \tag{5.7}$$

the closed-loop system will be stable.

From eqt. 5.7 we can also see why we want to model the uncertainty block into the block diagonal form, i.e., the structured uncertainties. For a block diagonalized uncertainty matrix, the uncertainties are decoupled. Therefore, it is very easy and precise to bound the maximum singular value of the whole uncertainty blocks. It will yield accurate robust stability analysis and a less conservative control design.

The commonly used algorithm to identify the upper bound of μ, in eqt. 5.6, is called Osborne's method [28]. This method provides an algorithm to choose the diagonal scaling matrix D. Then we can tightly bound the upper bound of μ.

5.2.5 Assessing robust performance with μ analysis

Singular value performance requirements can be combined with Δ-block robustness requirements in the μ analysis framework. Consider Fig. 5.3, let's require that the

maximum singular values of the closed-loop frequency response matrices between various inputs n and outputs y lie below given curves, e.g, $\gamma(\omega)$. we can simply multiply those outputs by $1/\gamma(\omega)$, perform the μ analysis, and consider the gain between the performance inputs and outputs as another Δ_p-block which is appended to those diagonal entries in the Δ-block of robust stability analysis. Let's call the system matrix of robust stability analysis as M_1 and the system considering both robust stability and performance as M_2. Therefore, if the system satisfies the robust stability criteria, then $\mu(M_1) < 1$. The performance criteria is satisfied if $\mu(M_2) < 1$

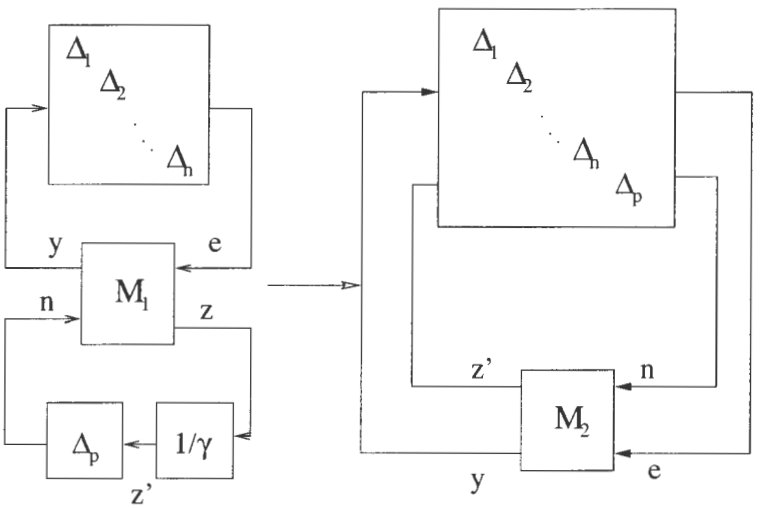

Figure 5.3 Assessing robust performance

5.2.6 Using H_∞ for μ synthesis

5.2.6.1 Algorithm

The μ synthesis is a two-step iterative process called D-K iteration:

1. Pick a diagonal $D(s)$ so that $D(s)$ and $D^{-1}(s)$ are stable, and so the upper bound of $\bar{\sigma}(DMD^{-1})$ is approximately minimized over the frequency range. Whenever

possible, pick constant D elements so that the number of controller states is unaffected. In the basic approach, we try to find a constant matrix D in each frequency point. After the calculation of all the $D(s)$ in the frequency range of concern, we approximate D with constants or with a low-order transfer function. On the first iteration, when K is unknown, we simply use $D = I$.

2. Use H_∞ synthesis to find a controller $K(s)$ which minimizes the scaled system's norm $\| DMD^{-1} \|$. Go back to step 1 and repeat until $\mu(M) < 1$ for all frequencies in the range or until no further reduction in μ achieved.

5.2.6.2 H_∞ controller design

Because the μ synthesis requires the synthesis of a H_∞ controller that satisfies $\| M \|_\infty < \gamma$ in each iteration, where γ is some positive scalar, we need to introduce the basic idea of H_∞ controller design.

Consider the diagram in Fig. 5.4, where the plant $P = \left[\begin{array}{c|cc} A & B_1 & B_2 \\ \hline C_1 & D_{11} & D_{12} \\ C_2 & D_{21} & D_{22} \end{array}\right]$ and K is the control loop. The diagram is known as a linear fractional transformation (LFT). The resulting closed loop transfer function from ω to z is denoted by $T_{z\omega} = F_l(P, K)$. The aim of H_∞ synthesis is to design the controller K such that the infinite norm of the closed-loop system is internally stable and $\| T_{z\omega} \|_\infty < \gamma$ if such a controller exists.

The following assumptions are made about the system P:

1. (A, B_2) is stabilizable and (C_2, A) is detectable.

2. D_{12} has full column rank and D_{21} has full row rank.

3. $\begin{bmatrix} A - j\omega I & B_2 \\ C_1 & D_{12} \end{bmatrix}$ has full column rank for all ω.

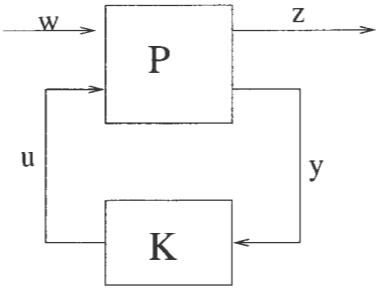

Figure 5.4 General diagram for controller design

4. $\begin{bmatrix} A - j\omega I & B_1 \\ C_2 & D_{21} \end{bmatrix}$ has full row rank for all ω.

The detailed equations of H_∞ synthesis can be found in [29].

5.2.6.3 Why choose μ synthesis instead of H_∞ synthesis

The μ synthesis requires the design of H_∞ controller in each iteration. One may ask what is the significance of μ synthesis? Taking H_∞ control means minimizing the infinity norm of the closed-loop transfer function from only one vector input to only one vector output. This limitation makes it difficult to achieve specified robustness margins simultaneously at the inputs and outputs of a MIMO system.

For the power system controller design, if an increase (or decrease) in an uncertainty parameter degenerates the system, e.g, an increase of load level destabilizes one or more modes, we can do H_∞ synthesis at the worst condition. The controller is consequently assumed robust because the uncertainty parameter can never be more sever than that for which the design is done. But if the 'direction' on the system of the effect of the uncertainty parameter change is not guaranteed, i.e., if we can not ensure that the design condition is in fact "worst case", then we have to choose another approach. One attractive approach is to bound these uncertainties one by one, from above and below,

and allow them to change in any direction simultaneously; this is known as μ synthesis.

5.3 Uncertainty modeling

The linearized power system equation in eqt. 3.28 can be expressed as:

$$\begin{aligned} \Delta\dot{X}_1 &= J_{11}\Delta X_1 + J_{12}\Delta X_2 + J_{13}\Delta u \\ 0 &= J_{21}\Delta X_1 + J_{22}\Delta X_2 + J_{23}\Delta u \end{aligned} \tag{5.8}$$

where $J_{11} = \frac{\partial f}{\partial X_1}$, $J_{12} = \frac{\partial f}{\partial X_2}$, $J_{13} = \frac{\partial f}{\partial u}$, $J_{21} = \frac{\partial g}{\partial X_1}$, $J_{22} = \frac{\partial g}{\partial X_2}$, $J_{23} = \frac{\partial g}{\partial u}$. When we assume the operating point remains the same, the direct influence of uncertainties in load model is the relation between P (or Q) and V. Since we choose the set of network equations as eqt. 3.14 as the bus real or reactive power injection, J_{22} the matrix that reflect the relation of P (or Q) and V. Therefore, only J_{22} is directly influenced by the nonlinear static load model when the operating point does not change. The indirect influence on the state equations is implemented through the coupled equations in eqt. 5.8. We may rewrite eqt. 4.4 for active load as:

$$P_{Li} = P_{Li0}[k_{i1}V_i^2 + k_{i2}V_i + k_{i3}] \tag{5.9}$$

where $k_{i1} = \frac{p_1}{V_{i0}^2}$, $k_{i2} = \frac{p_1}{V_{i0}}$, $k_{i3} = p_3$. Equation of similar format can be derived for reactive power. Therefore, we limit our discussion in the remaining of this section to real load. And we can derive the equations for reactive in the same format. The linearization at the operating point is:

$$\frac{\partial P_{Li}}{\partial V_i} = P_{Li0}[2k_{i1}V_i + k_{i2}] \tag{5.10}$$

Assume there are some uncertainties ${}_\Delta k_{ij}$ in k_{ij}, and such uncertainties only affect the load composition without changing the load level, i.e., the network solution remain the

same. Then:

$$\begin{aligned} \frac{\partial P_{Li}}{\partial V_i} &= P_{Li0}[2k_{i1}V_i + k_{i2}] \\ &+ P_{Li0}[2_{\Delta}k_{i1}V_i + {}_{\Delta}k_{i2}] \end{aligned} \tag{5.11}$$

From eqt. 4.4, if there is some uncertainty in the coefficients of static load representation, it will only affect the part that relates P_{Li} to. V_i, i.e., the $\frac{\partial P_{Li}}{\partial V_i}$ in J_{22}. Then J_{22} with uncertainties in active load can be expressed as:

$$\bar{J}_{22} = J_{22} + acd^T \tag{5.12}$$

where:

$\bar{J}_{22}$ is the new J_{22} matrix due to the changes in static load model.

$a = 2_{\Delta}k_{P1}V_i + {}_{\Delta}k_{P2}$

$c = [0, 0, \cdots, 0, -P_{li0}, 0, \cdots, 0]$ is a vector where -1 corresponds to the position of P_{Li} in network equations and elsewhere are zeros.

$d = [0, 0, \cdots, 0, 1, 0, \cdots, 0]$ is a vector where 1 corresponds to the position of V_i in the X_2 vector in network equations and elsewhere are zeros.

Using the Matrix Inversion Lemma, we know that

$$\begin{aligned} \bar{J}_{22}^{-1} &= (J_{22} + acd^T)^{-1} \\ &= J_{22}^{-1} - J_{22}^{-1}c(1 + ad^T J_{22}^{-1}c)^{-1}ad^T J_{22}^{-1} \end{aligned} \tag{5.13}$$

Using $\bar{J_{22}}^{-1}$ and substituting J_{ij}s, defined at the beginning of this section, into eqt. 3.31, the new A matrix is

$$\begin{aligned} \bar{A} &= J_{11} - J_{12}(\bar{J}_{22})^{-1}J_{21} \\ &= J_{11} - J_{12}(J_{22})^{-1}J_{21} \\ &+ J_{12}J_{22}^{-1}c(1 + ad^T J_{22}^{-1}c)^{-1}ad^T J_{22}^{-1}J_{21} \\ &= A + A_{\Delta} \end{aligned} \tag{5.14}$$

where A is the original A matrix and A_Δ is the change of A matrix due to the uncertainties.

Referring to the feedback loop in Fig. 5.2, if $M = \left|\begin{array}{c|c} A & B \\ \hline C & D \end{array}\right|$ is the state space description of the nominal plant model as in eqt. 3.16, then the closed-loop A matrix with uncertainties connected as in Fig. 5.2, is:

$$\bar{A} = A + B[1 - \Delta D]^{-1}\Delta C \tag{5.15}$$

Comparing eqt. 5.14 with eqt. 5.15,

$$\begin{aligned} \Delta &= a \\ B &= -J_{12}J_{22}^{-1}c \\ C &= -d^T J_{22}^{-1} J_{21} \\ D &= -d^T J_{22}^{-1} c \end{aligned} \tag{5.16}$$

the closed-loop A matrix will be the identical as eqt. 5.14. Comparing with eqt. 3.31 and eqt. 3.35, the A, B, C, D matrix can be achieved when we assume $y =_\Delta Vi$ and $e =_\Delta P_i$. This relation can be understood as that the nonlinear static load can be considered as a feedback loop from the bus voltage to bus load. We can obtain similar equations for reactive power as from 5.9 to 5.11,

5.4 Determination of uncertainties

The parameters which serve as uncertainties need to be independent. Intuitively we may choose ${}_\Delta k_{ij}$. But such parameters are constrained by

$$\begin{aligned} k_{i1}V_i^2 + k_{i2}V_i + k_{i3} &= 1 \\ k_{ij} + {}_\Delta k_{ij} &\geq 0 \\ k_{ij} &\geq 0 \end{aligned} \tag{5.17}$$

i.e. the sum of coefficients p_i or q_i are equal to one where i denotes the bus number of loads and $j = 1, 2, 3$. Therefore, we can not choose each ${}_{\Delta}k_{ij}$ as the uncertainties. Notice that in eqt. 5.12, if we choose

$$ {}_{\Delta}K \quad = \quad a = 2{}_{\Delta}k_{i1}V_i + {}_{\Delta}k_{i2} \tag{5.18} $$

as the uncertainties in bus i, we can express the impact of these uncertainties on the system in the form as in Fig.5.2 and these ${}_{\Delta}K_i$s constitute the diagonal elements in Δ block in Fig. 5.2.

Because of eqt.5.17, the ${}_{\Delta}k_{ij}$s are constrained., and these ${}_{\Delta}K_i$s are also constrained. From eqt. 5.18, the upper bound of ${}_{\Delta}K_i$ can be achieved when ${}_{\Delta}k_{i1}$ achieves its maximum positive change, i.e.,

$$ \begin{aligned} k_{i1} + {}_{\Delta}k_{i1} &= \frac{1}{V_i^2} \\ k_{i2} + {}_{\Delta}k_{i2} &= 0 \\ k_{i3} + {}_{\Delta}k_{i3} &= 0 \end{aligned} \tag{5.19} $$

Substituting eqt. 5.19 into eqt.5.18, the upper bound of ${}_{\Delta}K_i$ at bus i is $K_{ui} = frac2V_{i0} - 2k_{i1}V_{i0} - k_{i2}$.

The lower bound is obtained when ${}_{\Delta}k_{i1}$ and ${}_{\Delta}k_{i2}$ reaches its maximum negative change, i.e.,

$$ \begin{aligned} k_{i1} + {}_{\Delta}k_{i1} &= 0 \\ k_{i2} + {}_{\Delta}k_{i2} &= 0 \\ k_{i3} + {}_{\Delta}k_{i3} &= 1 \end{aligned} \tag{5.20} $$

Therefore, the lower bound of ${}_{\Delta}K_i$ at bus i is $K_{li} = -2k_{i1}V_{i0} - k_{i2}$. So:

$$ -2k_{i1}V_{i0} - k_{i2} \leq {}_{\Delta}K \leq \frac{2}{V_{i0}} - 2k_{i1}V_{i0} - k_{i2} \tag{5.21} $$

We will use eqt. 5.21 in the controller synthesis.

By μ analysis, we can calculate the range of the smallest "destablizing" uncertainties. From eqt. 5.7 we notice that $\bar{\sigma}(\Delta) = max(_{\Delta}K_i) > \frac{1}{\mu(M)}$ will destabilize the system. When we have the bound of μ as $\mu_l \leq \mu \leq \mu_u$ from eqt. 5.6, the bound on $_{\Delta}K_i$ is $\frac{1}{\mu_l} \geq {}_{\Delta}K_i \geq \frac{1}{\mu_u}$. Therefore, the lower bound $\frac{1}{\mu_u}$ gives the maximum change in $_{\Delta}K_i$s that can still maintain the stability, while the upper bound $\frac{1}{\mu_u}$ gives the minimum value in $_{\Delta}K_i$s that the system is guaranteed to be unstable. Because $_{\Delta}K_i$ is the composition of $_{\Delta}k_{i1}$ and $_{\Delta}k_{i2}$, one would like to know what is the corresponding load composition in terms of constant impedance, constant current, and constant power. We may calculate backward for the possible value of $_{\Delta}k_{ij}$. Since the $_{\Delta}k_{ij}$s are solutions of eqt. 5.17 and eqt. 5.18. In these equations with only $_{\Delta}K_i$ specified, there are two equations and three unknowns. Therefore the solutions are not unique. What follows is one possible solution. We divide the range of $_{\Delta}K_i$ into 4 intervals, from the lower bound to the upper bound. It gives a physical understanding that for what proportion of load composition that can cause the instability of system. Later we will use these calculation to show the correctness of the uncertainty modeling.

1. when $_{\Delta}k_{i1} + k_{i1} = 0$, then $-2k_{i1}V_{i0} - k_{i2} \leq {}_{\Delta}K < -2V_{i0}k_{i1}$,
   where $_{\Delta}k_{i1} = -k_{i1}$ and $_{\Delta}k_{i2} = {}_{\Delta}K + 2V_{i0}k_{i1}$.

2. when $_{\Delta}k_{i2} = 0$, then $-2k_{i1}V_{i0} \leq {}_{\Delta}K < 0$,
   where $_{\Delta}k_{i1} = -\frac{{}_{\Delta}K}{2V_{i0}}$.

3. when $_{\Delta}k_{i2} = -{}_{\Delta}K$, then $0 \leq {}_{\Delta}K \leq k_{i2}$
   where $_{\Delta}k_{i1} = \frac{{}_{\Delta}K}{V_0}$.

4. when $_{\Delta}k_{i2} + k_{i2} = 0$, then $k_{i2} < {}_{\Delta}K \leq \frac{2}{V_{i0}} - 2k_{i1}V_{i0} - k_{i2}$
   $_{\Delta}k_{i1} = \frac{{}_{\Delta}K + k_{i2}}{2V_{i0}}$ and $_{\Delta}k_{i2} = -k_{i2}$

and $_{\Delta}k_{i3} = 1 - {}_{\Delta}k_{i2}V_{i0} - {}_{\Delta}k_3V_{i0}^2$ for all the cases.

5.5 Control implementation of μ synthesis

The diagram for μ synthesis is shown in Fig. 5.6. Here we introduce some new blocks in order to implement the μ synthesis. The uncertainty block, as in Fig. 5.2, having diagonal elements defined in eqt. 5.18, are implemented with 3 diagonal matrices as Δ, W_t and W_b block. The elements in W_t and W_b are defined as:

$$W_{ti} = \frac{2}{K_{ui} - K_{li}} \tag{5.22}$$

$$W_{bi} = \frac{K_{ui} + K_{li}}{2} \tag{5.23}$$

where K_u and K_l are upper and lower bound of ${}_{\Delta}K_i$ defined in eqt. 5.21. By this transformation of eqt. 5.22 and 5.23, we transfer the ${}_{\Delta}K_i$ as in eqt. 5.21 to Δ_i with boundary of $|\Delta_i| \leq 1$.

We also introduce a performance weighting block W_p. The input is the change in real power of the line TCSC is installed, and the output is the change in susceptance for the same line, i.e., the performance requirement is the gain of the controller should be below $1/W_p$. Because the goal of this controller is to damp low frequency oscillations, we would like the controller to have larger gain at low frequency and smaller gain at high frequency. It will minimize the impact of this controller on other high frequency modes. Here we choose $W_P = 0.01\frac{s+10}{s+100}$. The bode plot of $1/W_p$ is given in Fig. 5.5.

5.6 Numerical example

5.6.1 Impact of load composition

The same 3-area, 6-machine sample system which is illustrated in chapter 4 is used to illustrate the μ analysis and synthesis. The TCSC's fixed compensation level is set to 40%. Stressing the system by increasing the load at bus #10 to 450MW and generation at bus #6, the two interarea modes become critical. The effect of load representation

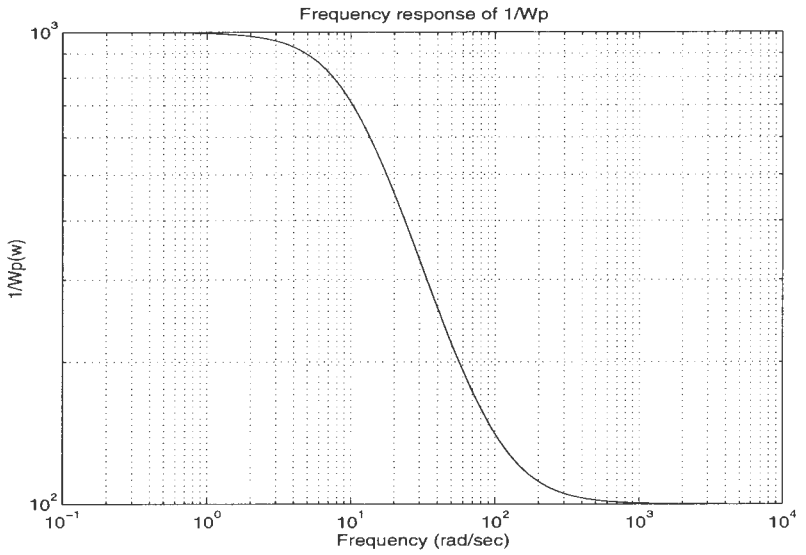

Figure 5.5 Performance requirement

of all the load bus vs. these two eigenvalues are listed in Table 5.1. Here the load composition of each load bus change simultaneously.

It is shown in Table 5.1 that load composition has great influence on system eigenvalues. It may make a well damped system ($\xi = 6.9944\%$) unstable ($\xi = -2.7174\%$). Moreover, the load modeling can have different impact on different modes. In this case, when the load model changes from 100 % constant impedance to 100 % constant power, mode 1 becomes unstable and mode 2 becomes more stable. Because there is substantial uncertainty in the accuracy of the load representation data, and because the system

Table 5.1 Interarea modes

Load Model(%)			Mode 1		Mode 2	
Z	I	P	$f(Hz)$	$\xi(\%)$	$f(Hz)$	$\xi(\%)$
100	0	0	1.1401	6.9944	0.8935	0.1481
50	50	0	1.1191	5.9533	0.9020	0.4435
50	0	50	1.0954	4.2375	0.9118	0.7918
0	50	50	1.0701	1.4984	0.9209	1.0570
0	0	100	1.0457	-2.7174	0.9301	1.3221

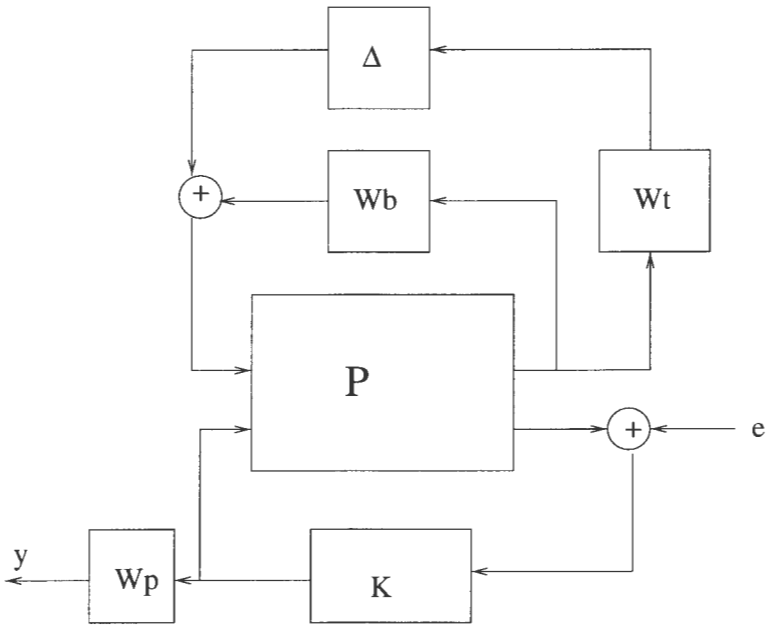

Figure 5.6 Block diagram for μ synthesis

stability degrades as we change load representation data in either "direction", we are not guaranteed to find the worst condition, so that we can not synthesis the H_∞ for the worst cases. It is quite suitable to use μ in the controller design.

5.6.2 Correctness of modeling

In order to validate our uncertainty modeling above, we assume the uncertainties exist only in one bus #9. From experience we know that the uncertainties in one bus will not dramatically affect the stability of the system, so we stress the system little bit more as load at bus #10 by increasing the active load to 470MW. The initial composition of all load is 100% constant impedance for both real and reactive power. The μ curves, for the frequency range of all modes, are shown in Fig. 5.7.

Since the μ value is computed only for discrete frequency values, the accuracy of μ

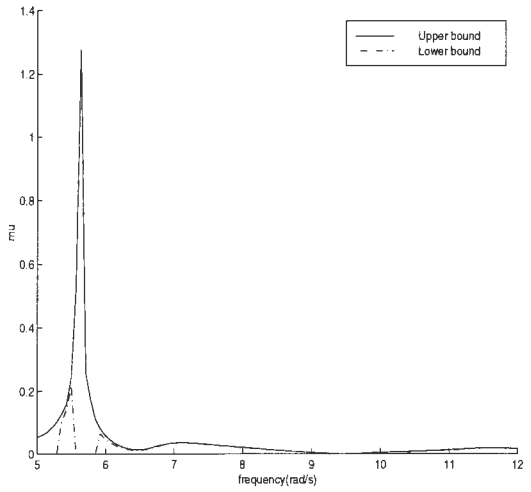

Figure 5.7 μ curve for all modes

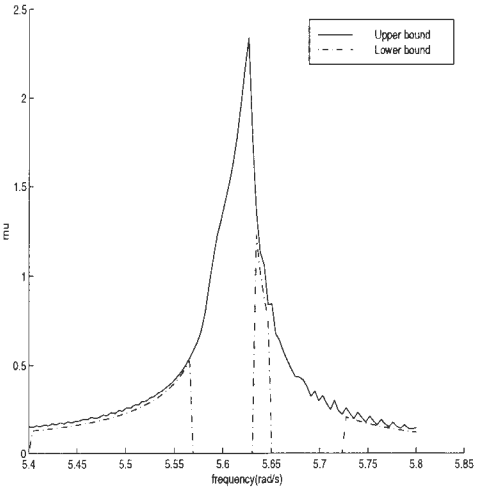

Figure 5.8 μ The critical mode

analysis depends heavily on the resolution of the frequency. The μ curves for the critical mode of high resolution is shown as Fig. 5.8. Comparing Fig. 5.7 and Fig. 5.7 we notice that Fig. 5.7 shows the peak μ is about 1.3, instead of the more accurate value of 2.4 in Fig. 5.8. Fig. 5.7 fails to show the critical mode accurately because of the low resolution of frequency. Since ${}_{\Delta}K_i$ are real uncertainties. But for current algorithm, we can not calculate the lower bound. So the lower bound in Fig. 5.7 and Fig. 5.8 are not accurate.

The frequency corresponding to the peak value of upper bound of μ is $\omega = 5.6273$ and the $\mu = 2.3556$. Since the uncertainty matrix Δ is diagonal, the singular values are ${}_{\Delta}K_i$ for real and reactive power respectively. Therefore, the smallest value of ${}_{\Delta}K_i$ that makes the system close to zero damping is: $|{}_{\Delta}K_i| = 1/\mu = 0.4246$ for either real or reactive load. We calculate backward for the possible change of ${}_{\Delta}k_{i1} = 0.42167$ and ${}_{\Delta}k_{i2} = -0.42452$, i.e., 92.74 % constant impedance and 6.25% constant current. Substitution of these values for real and reactive power respectively into a small signal stability program yields that the critical eigenvalue is $-7.9065 \times 10^{-5} \pm j5.6261$ which is very close to instability. This shows that μ analysis gives very close estimation of the

smallest destabilizing uncertainties. It also shows the effectiveness of the uncertainties modeling.

5.6.3 Controller synthesis

By applying the D-K iteration procedure as in section 5.2.6.1, we obtain the μ controller, which is comprised of 48 states. Using balanced system reduction [18], we find there is a sunddent drop of Hankel norm value between 4th and 5th elements. We choose a controller of 4 states. The frequency response of the reduced controller and the original one is shown in Fig. 5.9. It shows that $4th$ order controller is a very good approximation of the higher order one.

We would like to check first if our design goal, which is to design the controller to stabilize the system and the closed loop system satisfies the performance criteria, is satisfied by doing mu analysis on the robust stability and performance in Fig. 5.10 and 5.11. The μ plot for robust stability is computed only considering the uncertainty block as in Fig. 5.6. The robust performance is calculated when we consider another uncertainty block connecting y and e as in Fig. 5.6, and this block is append diagonally to the uncertainty block for stability. The peak μ for both robust stability and robust performance are less than one. Since $|\Delta_i| \leq 1$, so the closed loop system satisfies our design requirement for robust stability and robust performance.

The controller effectiveness can also be studied by comparing the performance of controller designed by the residue method and that designed by μ synthesis. We do this for the same operating condition as in section 4.4.2. The results for this comparison are shown in Table 5.2 (mode 1) and Table 5.3 (mode 2). Although Table 5.2 indicates that mode 1 is not damped as well by the μ controller as by the residue controller, we see that both controller do stabilize mode 1 for all values of load representation data. In Table 5.3, however, we see that the residue controller did not stabilize mode 2 for the constant power case, but the μ controller did. This we see that in using μ, for this

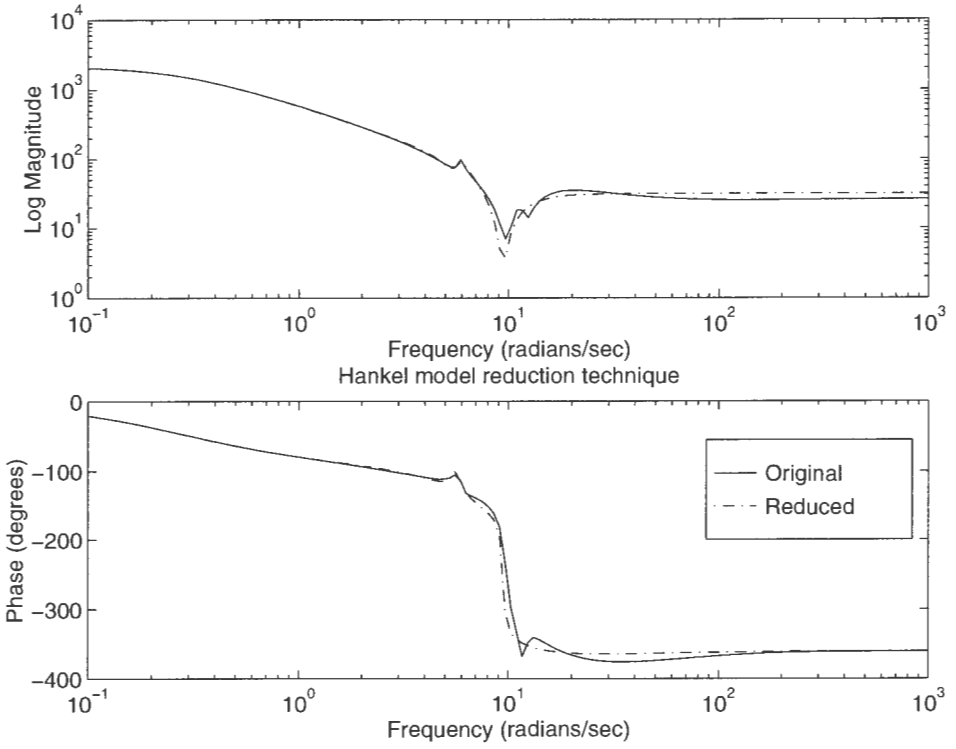

Figure 5.9 Reduced controller

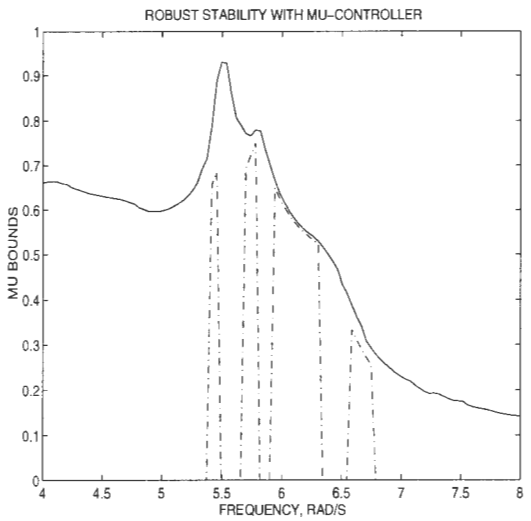

Figure 5.10 μ for robust stability

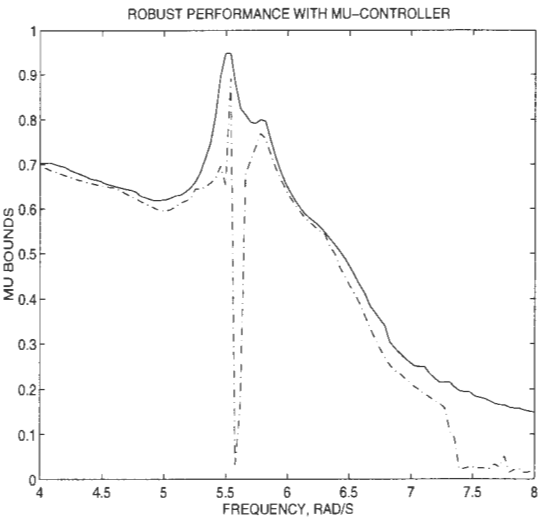

Figure 5.11 μ for robust performance

Table 5.2 Controller performance for interarea modes under different load modeling (Mode 1)

Load Models			Original		μ		Residue	
Z	I	P	$f(Hz)$	$\xi\%$	$f(Hz)$	$\xi\%$	$f(Hz)$	$\xi\%$
100	0	0	0.8745	1.2493	0.8651	0.9006	0.9325	38.8750
50	50	0	0.8856	-0.9510	0.8771	2.2545	0.8822	41.8090
50	0	50	0.8974	-0.6560	0.8755	3.8111	0.8414	43.1570
0	50	50	0.9111	-0.2820	0.8697	4.7002	0.8125	43.1590
0	0	100	0.9243	0.6522	0.8611	5.6329	0.7959	42.0960

instance, accepted diminished damping for mode 1 in turn of robust control for both modes.

5.7 Conclusion

The work of μ analysis in this chapter has modeled the uncertainties in load composition into structured uncertainties. Because the uncertainty affects the system linearly, our reduced ordered controller of order 4 has very good approximation of the higher order one. This controller has better robust performance compared with the controller designed from residue.

Table 5.3 Controller performance for interarea modes under different load modeling (Mode 2)

Load Models			Original		μ		Residue	
Z	I	P	$f(Hz)$	$\xi\%$	$f(Hz)$	$\xi\%$	$f(Hz)$	$\xi\%$
100	0	0	1.1212	6.7240	0.9026	4.7903	0.9553	10.909
50	50	0	1.0951	5.4225	0.9053	3.9818	0.9625	8.3966
50	0	50	1.0648	3.2133	0.9186	3.0112	0.9653	5.8797
0	50	50	1.0305	-0.513	0.9364	2.7912	0.9648	3.1007
0	0	100	0.9972	-0.702	0.9574	2.7431	0.9615	-0.355

Several characteristics of the uncertainties in load modeling make it suitable for μ analysis:

1. The uncertainty affects the system linearly. So there is no approximation when we form the structured uncertainty matrix;

2. The changes in static load modeling can either stabilize or degenerate the system modes. We are not guaranteed to find the worst case, so that we can not synthesis H_∞ at the worst case and make the controller have a better robustness for less critical situation.

3. The frequency of concern is between 1 rad/s to 10 rad/s. More, from chapter 4 we know that TCSC has lower impact on higher frequency oscillation. So we can limit our study to this narrow frequency range. It is easy to achieve higher resolution.

The major problem of μ analysis and synthesis is that there is a large amount of calculation. Moreover, it can be difficult to model as structured uncertainties variation in other common parameter such as load level and topology change.

CHAPTER 6 CONCLUSIONS

The objective of this thesis is to design a controller for Thyristor Controlled Series Compansator (TCSC) to damp intereare oscillations. The behavior of TCSC is studied and a controller is designed by the residue method. Then the robustness issue is discussed by comparing TCSC and PSS. The structured uncertainties in load representation is studied, and μ synthesis is used to design the controller with the consideration of the uncertainties. The following conclusion can be drawn:

- The TCSC can be modeled as a varying impedance with one time constant when it is considered to static stability study.
- Functional sensitivity, i.e., the residue method can be used to:
  - Determine the best location of TCSC.
  - Design the power system damping controller with different input/output pairs by pole placement. Since the nonlinearity of power system, the desired damping ratio may be different from the real one.
- TCSC has more global influence on the power system stability than PSS. Also TCSC is more vulnerable to the change of operating conditions and uncertainties in system parameters.
- The uncertainties in load representation can be modeled into structured uncertainties. When these uncertainties is considered in μ synthesis, the controller has

similar damping performance over the range of uncertainty changes. The controller designed by residue method is simple and has very good performance for the designate operating point, and a good robustness. While the μ approach has the potential to improve the damping with the consideration of several modes and under different operating point. Since the uncertainty modeling is crucial to μ approach, we will emphasize on it in future research.

APPENDIX A NETWORK DATA

Table A.1 Bus data of the sample system

bus number	voltage (pu)	angle (degree)	p_gen (pu)	q_gen (pu)	p_load (pu)	q_load (pu)	bus [1] _type	Name
1	1.05	0.00	0.90	0.30	0.00	0.00	2	gen #1
2	1.05	0.00	0.90	0.20	0.00	0.00	2	gen#2
3	1.05	0.00	0.80	0.20	0.00	0.00	2	gen#3
4	1.05	0.00	0.90	0.30	0.00	0.00	2	gen#4
5	1.05	0.00	0.90	0.20	0.00	0.00	2	gen#5
6	1.05	0.00	0.80	0.20	0.00	0.00	1	gen#6
7	1.00	0.00	0.00	0.00	3.00	1.00	3	load#1
8	1.00	0.00	0.00	0.00	0.30	-0.10	3	load#2
9	1.00	0.00	0.00	0.00	0.80	0.20	3	load#3
10	1.00	0.00	0.00	0.00	0.50	0.00	3	load#4
11	1.00	0.00	0.00	0.00	0.40	0.10	3	load#5
12	1.00	0.00	0.00	0.00	0.00	0.00	3	
13	1.00	0.00	0.00	0.00	0.00	0.00	3	
14	1.00	0.00	0.00	0.00	0.00	0.00	3	
15	1.00	0.00	0.00	0.00	0.00	0.00	3	

Table A.2 Line parameters data of the sample system

from bus	to bus	resistance(pu)	reactance(pu)	line charging(pu)	tap ratio
1	2	0.010	0.10	0.000	0
2	7	0.005	0.05	0.005	0
7	8	0.010	0.10	0.010	0
8	12	0.005	0.05	0.000	0
12	9	0.050	0.50	0.500	0
9	4	0.010	0.10	0.000	0
4	3	0.010	0.10	0.000	0
8	10	0.010	0.10	0.010	0
10	11	0.080	0.80	0.080	0
11	6	0.010	0.10	0.000	0
6	5	0.010	0.10	0.000	0
10	13	0.000	-0.32	0.000	0
11	13	0.080	0.80	0.080	0

APPENDIX B GENERATOR DATA

Table B.1 Machine parameters data of the sample system

machine number	#1 to #6
machine base mva	900
leakage reactance x_l(pu)	0.2
resistance r_a(pu)	0.0
d-axis sychronous reactance x_d(pu)	1.8
d-axis transient reactance $x_d^{'}$(pu)	0.3
d-axis subtransient reactance $x_d^{"}$(pu)	0.25
d-axis open-circuit time constant $T_{do}^{'}$(sec)	8.0
d-axis open-circuit subtransient time constant $T_{do}^{"}$(sec)	0.03
q-axis sychronous reactance x_q(pu)	1.7
q-axis transient reactance $x_q^{'}$(pu)	0.55
q-axis subtransient reactance $x_q^{"}$(pu)	0.25
q-axis open-circuit time constant $T_{qo}^{'}$(sec)	0.4
q-axis open circuit subtransient time constant $T_q o^{"}$(sec)	0.05
inertia constant H(sec)	3.5
damping coefficient d_o(pu)	5
dampling coefficient d_1(pu)	0

Table B.2 Exciter parameters data of the sample system

exciter type	IEEE-30
machine number	#1 to #6
input filter time constant T_R	0.0
voltage regulator gain K_A	100
voltage regulator time constant T_A	0.01
voltage regulator time constant T_B	10
voltage regulator time constant T_C	1
maximum voltage regulator output V_{Rmax}	5
minimum voltage regulator output V_{Rmin}	-5

BIBLIOGRAPHY

[1] Narain G. Hingorani, "FACTS flexible AC Transmission System," *The Second Annual Transmission and Wheeling Conference*, November 1991.

[2] G. Juette, P. Luetzelberger, A. Schultz, S. McKenna, and D. Torgerson, "Advanced series compensation (ASC) main circuit and related components," *Proc. of FACTS Conference 2*, pp. 3.4–1 to 3.4–13, December 1992.

[3] J. Urbanek, R. Piwko, D. McDonald, and N.Artinez, "Thyristor controlled sereis compensation – equipemnt design for the slatt 500 kv installation," *Proc. of FACTS Conference 2*, pp. 3.1–1 to 3.1–19, December 1992.

[4] CIGRE working group 14.18, "Thyristor controlled series compensation." Draft.

[5] J. Paserba, N. Miller, E. Larsen and R. Piwko, "A thyristor controlled series compensation model for power system stability analysis," *IEEE Transactions on Power Delivery*, vol. 10, pp. 1471–1478, July 1995.

[6] S.G. Helbing and G.G. Karady, "Investigations of an advanced form of series compensation," *IEEE Transactions on Power Delivery*, vol. 9, pp. 939–947, April 1994.

[7] N. Christl, R. Hedin, P.E. Krause and S.M. McKenna, "Advanced series compensation (asc) with thyristor controlled impedance," *CIGRE*, no. 14/37/38-05, 1992.

[8] P. Mattavelli, G.C. Verghese and A.M. Stankovic, "Phasor dynamics of thyristor-controlled series capacitor system." IEEE/PES Summer Meeting, Denver, Colorado, 1996.

[9] P.S. Dolan, J.R. Smith and W.A. Mittelstadt, "Study of TCSC optimal damping control parameters for different operating conditions," *IEEE Transactions on Power System*, vol. 10, pp. 1972–1978, November 1995.

[10] H.F. Wang and F.J. Swift, "A unified model for analysis of FACTS devices in damping power system oscillations part I: Single-machine infinite-bus power systems," *IEEE Transactions on Power Delivery*, vol. 12, pp. 941–946, April 1997.

[11] F.Luis Pagola, Ignacio J. Perez-Arriaga and George C. Verghese, "On sensivitivities, residues and participations: applications to oscillatory stability analysis and control," *IEEE Transactions on Power Systems*, vol. 4, pp. 278–285, Feburary 1989.

[12] E. Zhou, "Functional sensitivity concept and its application to power system," *IEEE Transactions on Power Systems*, vol. 9, pp. 518–524, February 1994.

[13] N. Martins, "Oscillation damping analysis and control studies of the future interconnection between the north-northeast and south-southeast systems." V Symposium of Specialists in Electric Operational and Expansion Planning, May, 1996.

[14] M.E. Aboul-Ela, A.A. Sallam, J.D. McCalley and A.A. Fouad, "Damping controller design for power system oscillation using global signals," *IEEE Transactions on Power System*, vol. 11, pp. 767–773, May 1996.

[15] H.F. Wang and F.J. Swift, and M. Li, "Comparison of modal controllability between facts-based stabilizer and pss in increasing the oscillation stability of multimachine power system," *IEE Proc. of Generation, Transmission and Distribution*, pp. 575–581, November 1996.

[16] P. Kundur, *Power System Stability and Control.* McGraw-Hill Inc., New York, 1993.

[17] Y.V. Makarov, V.A. Maslennikov and D.J. Hill, "Revealing loads having the biggest influence on power system small disturbance stability," *IEEE Transactions on Power System*, pp. 2018–2023, November 1996.

[18] K. G. G.J. Balas, J.C. Doyle and R. S. A. Packard, *μ-analysis and synthesis toolbox.* The MathWorks, Inc., Natic, MA, 1993.

[19] M. Klein, L.X. Le, G.J. Rogers, S. Farrokhpay and N.J. Balu, "H_∞ damping controller design in large power systems," *IEEE Transactions on Power Systems*, pp. 158–166, February 1995.

[20] Q. Zhao and J. Jiang, "Robust svc controller design for improving power system damping," *IEEE Transactions on Power Systems*, pp. 1927–1932, November 1995.

[21] S.S. Ahmed, L. Chen and A. Petroianu, "Design of suboptimal H_∞ excitaton controllers," *IEEE Transactions on Power Systems*, pp. 312–318, February 1996.

[22] G.N. Taranto, J.H. Chow and H.A. Othman, "Robust decentralized control design for damping power system oscillation," *Proceeding of IEEE 33rd Conference on Decision and Control*, pp. 4080–4085, December 1994. Lake Buena, FL.

[23] S. Chen and O. Malik, "Power system stabilizer design using μ synthesis," *IEEE Transactions on Energy Conversion*, pp. 175–181, October 1995.

[24] Q. Liu, "Modal sensitivity analysis and TCSC effectiveness." Thesis for Master of Science, Iowa State University, 1996.

[25] E. Larsen, C. Bowler, B. Damsky and S. Nilsson, "Benefits of thyristor controlled series compensation." CIGRE 1992 joint section 14/37/38, Paris, August, 1992.

[26] Sasan G. Jalali, Ron A. Hedin, Macros Pereira and Kadry Sadek, "A stability model for the advanced series compensator (ASC)," *IEEE Transactions on Power Delivery*, vol. 11, pp. 1128–1137, April 1996.

[27] Prepared by General Electric Company, "Load modeling for power flow and transient stability computer studies," *EPRI Project 849-7*, January 1987.

[28] E.E. Osborne, "On preconditioning of matrices," *J. Assoc. Comp.*, pp. 338 – 345, March 1960.

[29] J. C.Doyle, K. Glover, P. Khargonekar and B. Francis, "State space solution to standard H_2 and H_∞ control problems," *IEEE Transactions Automatic Control*, August 1989.